Observations of speciated isoprene nitrates in Beijing: implications for isoprene chemistry

Claire E. Reeves[1], Graham P. Mills[1], Lisa K. Whalley[2], W. Joe F. Acton[3], William J. Bloss[4], Leigh R. Crilley[4,5], Sue Grimmond[6], Dwayne E. Heard[7], C. Nicholas Hewitt[3], James R. Hopkins[8], Simone Kotthaus[6,9], Louisa J. Kramer[4], Roderic L. Jones[10], James D. Lee[8], Yanhui Liu[1], Bin Ouyang[10], Eloise Slater[7], Freya Squires[11], Xinming Wang[12], Robert Woodward-Massey[13], and Chunxiang Ye[13]

[1]Centre for Ocean and Atmospheric Sciences, School of Environmental Sciences, University of East Anglia, UK
[2]National Centre for Atmospheric Science, School of Chemistry, University of Leeds, UK
[3]Lancaster Environment Centre, Lancaster University, Lancaster, UK
[4]School of Geography, Earth and Environmental Sciences, the University of Birmingham, Birmingham, B15 2TT, UK
[5]now at Department of Chemistry, York University, Toronto, Canada.
[6]Department of Meteorology, University of Reading, Reading, UK
[7]School of Chemistry, University of Leeds, UK
[8]National Centre for Atmospheric Science, Wolfson Atmospheric Chemistry Laboratories, Department of Chemistry, University of York, UK
[9]Institut Pierre Simon Laplace, Ecole Polytechnique, France
[10]Department of Chemistry, University of Cambridge, UK
[11]Wolfson Atmospheric Chemistry Laboratories, Department of Chemistry, University of York, UK
[12]Guangzhou Institute of Geochemistry, Chinese Academy of Sciences, Guangzhou, China
[13]Beijing Innovation Center for Engineering Science and Advanced Technology, State Key Joint Laboratory for Environmental Simulation and Pollution Control, Center for Environment and Health, College of Environmental Sciences and Engineering, Peking University, Beijing, 100871, China

Correspondence to: Claire E. Reeves (c.reeves@uea.ac.uk)

Abstract. Isoprene is the most important biogenic volatile organic compound in the atmosphere. Its calculated impact on ozone (O_3) is critically dependent on the model isoprene oxidation chemical scheme, in particular the way the isoprene-derived organic nitrates (IN) are treated. By combining gas chromatography with mass spectrometry, we have developed a system capable of separating, and unambiguously measuring, individual IN isomers. In this paper we report measurements from its first field deployment, which took place in Beijing as part of the Atmospheric Pollution and Human Health in a Chinese Megacity (APHH-Beijing) programme. Seven individual isoprene nitrates were identified and quantified during the summer campaign: two β-isoprene hydroxy nitrates (IHN); four δ isoprene carbonyl nitrates (ICN); and propanone nitrate. Box model simulations using the Master Chemical Mechanism (MCM) (v.3.3.1) were made to assess the key processes affecting the production and loss of the IN.

The observed mixing ratios of the two β-IHN are well correlated with an R^2 value of 0.85. The mean for their ratio ((1-OH, 2-ONO_2)-IHN : (4-OH, 3-ONO_2)-IHN) is 3.4 (the numbers in the names indicate the carbon (C) atom in the isoprene chain to which the radical is added). This observed ratio tends to increase with decreasing mixing ratios of nitric oxide (NO),

although the relationship is weak due to there being only a few data points. Examining this relationship in a box model demonstrates that it is largely a reflection of the respective β-IHN precursor peroxy radicals which, at NO mixing ratios of less than 1 part per billion (ppb) shift towards those of (1-OH, 2-ONO_2)-IHN. The model, however, tends to simulate lower ratios than observed.

Of the δ-ICN, the two *trans* (E) isomers are observed to have the highest mixing ratios and the mean isomer ratio (E-(4-ONO_2, 1-CO)-ICN to E-(1-ONO_2, 4-CO)-ICN)) is 1.4, which is considerably lower than the expected ratio of 6 for addition of NO_3 in the C1 and C4 carbon positions in the isoprene chain. The model produces far more δ-ICN than observed, particularly at night and it also simulates an increase in the daytime δ-ICN that greatly exceeds that seen in the observations. Interestingly, the modelled source of δ-ICN is predominantly during the daytime, due to the presence in Beijing of appreciable daytime amounts of NO_3 along with isoprene. δ-ICN is modelled to be the main precursor for propanone nitrate, but their modelled ratio is very different from the observed. The model also simulated large enhancements of (1-OH, 4-ONO_2)-IHN and δ-ICN on some nights, but we did not observe these enhancements in δ-ICN and, despite the modelled mixing rations of (1-OH, 4-ONO_2)-IHN being above our detection limit, we did not detect it.

This study demonstrates the value of speciated IN measurements to test our understanding of the isoprene degradation chemistry. Our interpretation is limited by the uncertainties in our measurements and relatively small data set, but highlights areas of the isoprene chemistry that warrant further study, in particular the impact of NO on the formation of the β-IHN, and the NO_3 initiated isoprene degradation chemistry.

1 Introduction

Isoprene is the most important biogenic volatile organic compound (BVOC) in the atmosphere, with its emissions accounting for around 500 Tg yr^{-1}, about half of the global biogenic non-methane VOC emissions (Guenther et al., 2012). It is emitted by vegetation primarily during the daytime as a function of temperature and solar radiation and is readily oxidised by the hydroxyl (OH) and nitrate (NO_3) radicals and ozone (O_3). Through its degradation chemistry, isoprene impacts O_3 and the formation of secondary organic aerosols (SOA), which together impact the oxidising capacity of the atmosphere and radiative forcing. Global and regional model studies show that the calculated impact of isoprene on O_3 is critically dependent on the model isoprene oxidation chemical scheme, in particular the way the isoprene-derived nitrates (IN) are treated (e.g. Emmerson and Evans, 2009; Fiore et al., 2005; Squire et al., 2015; von Kuhlman et al., 2004; Wu et al., 2007; Bates and Jacob, 2019; Schwantes et al., 2020). Much of the uncertainty in this chemistry is related to the yield and fate of IN, in particular whether NO_X (nitrogen oxides) and radicals, which are tied up in the nitrates, are later recycled or lost from the atmosphere.

First generation IN are formed following oxidation of isoprene by either OH or NO_3 (Wennberg et al., 2018) (Fig. 1). On oxidation by OH, peroxy radicals are formed which when they react with nitric oxide (NO) can lead to the formation of hydroxy nitrates (IHN), with a yield of around 4-15 % (e.g. Chen et al., 1998; Chuong and Stevens, 2002). These are dominated by β-IHN, but some δ-IHN are also formed. Although NO_3 is mostly present at night, isoprene oxidation by NO_3 can be important, particularly in the early evening (Brown et al., 2009) and, due to the larger organic nitrate yield of ~65-80 % (Kwan et al., 2012; Perring et al., 2009b, Rollins et al., 2009; Schwantes et al., 2015), can be responsible for a considerable proportion (~40-50 %) of the IN (Horowitz et al., 2007; von Kuhlmann et al., 2004; Paulot et al., 2012; Xie et al., 2013). Depending on the fate of the peroxy radicals formed following NO_3 addition, a variety of IN can be produced: isoprene hydroperoxy nitrates (IPN); isoprene dinitrates (IDN); isoprene carbonyl nitrates (ICN); as well as IHN.

The fate of first generation IN is poorly understood and until recently understanding was based on theoretical calculations, with most observational constraints based on measurements of either groups of nitrates as totals, or degradation products that come from more than one reaction and precursor species (Giacopelli et al., 2005; Paulot et al., 2009; Rollins et al., 2009). Much advancement in recent years has been made through new laboratory studies following the synthesis of some of the IN (Jacobs et al., 2014; Lee et al., 2014; Lockwood, et al., 2010; Teng et al., 2017; Xiong et al., 2016), but these are still limited to specific IN isomers (six IHN and one ICN) and reaction rates for others are based on extrapolation and structural activity relationships. The IN are lost via reaction with OH, O_3 and NO_3 (Wennberg et al., 2018) and by photolysis (Xiong et al., 2016; Müller et al., 2014) and deposition (Nguyen et al., 2015), and have lifetimes of the order of a few hours.

One of the key issues is whether NO_X and radicals are returned to the system or whether they remain tied up in second generation nitrates. In the case of the IHN and ICN reactions with OH can lead to the formation of carbonyls and release of NO_2 or the formation of shorter chained nitrates such as methyl vinyl ketone nitrate, methacrolein nitrate, propanone nitrate (acetone nitrate) and ethanal nitrate, with the ratio between these two pathways differing for specific IN isomers (Wennberg et al., 2018). Critically the β-IHN and δ-IHN have different lifetimes and return different fractions of NO_2 (Paulot et al., 2012). As the yields of the IHN from the β and δ peroxy radicals are fairly similar (Teng et al., 2017), a key factor in the amount of NO_X recycled is the relative yields of the β and δ peroxy radicals from OH oxidation of isoprene.

Over the last decade or so there has been a considerable effort to improve understanding of isoprene oxidation mechanisms, with the latest understanding detailed in Wennberg et al. (2018) (hereafter referred to as W2018). More details of the chemistry of IN are given in Sect. 1 of the Supplementary Information (Supp. Info.).

The implications of this chemistry have been subject to several model studies (Fiore et al., 2005; Wu et al., 2007; Emmerson and Evans, 2009; Paulot et al., 2012; Xie et al, 2013; Squire et al., 2015; Bates and Jacob, 2019; Schwantes et al., 2020), although it should be noted that several of these studies predate many of the recent advancements in understanding of the

detailed isoprene nitrate chemistry outlined above. However, the key findings are that the yield of the IN and the rate at which NO_X is recycled are important in determining the overall impact of isoprene on O_3 and the distribution of O_3 production.

The results of the model studies need to be evaluated against field data of IN. Some of the early field measurements used gas chromatography (GC) to separate the IHN (Werner et al., 1999; Giacopelli et al., 2005; Grossenbacher et al., 2001; 2004), but without synthesised samples of the IN, the identity of the specific isomers could not be confirmed. Several studies (e.g. Horowitz et al., 2007; Perring et al., 2009a; Mao et al., 2013; Xie et al., 2013; Zare et al., 2018) have used thermal dissociation laser-induced fluorescence spectroscopy (TD-LIF) measurements of the sum of alkyl and multifunctional nitrates (∑ANs) as observational constraints, but whilst this includes IN, it also includes other organic nitrates, and there is no separation of individual IN. Field studies using chemical ionisation mass spectrometry (CIMS) (e.g. Beaver et al., 2012; Xiong et al., 2015; Fisher et al., 2016; Lee et al., 2016; Lee et al., 2018) were able to provide further insight through partial separation of different types of IN, including first generation and second generation IN, but were not able to distinguish between different isomers (e.g. of IHN).

By combining GC with mass spectrometry (MS), we (Bew et al., 2016; Mills et al., 2016), Vasquez et al. (2018) and Li et al. (2019) have developed systems capable of separating, and unambiguously measuring, individual IN isomers in the field. We used negative ion (NI) MS, whilst Vasquez et al. (2018) used CIMS and Li et al. (2019) EI-MS.

In this study we deploy our system in the field for the first time, allowing us to quantify the concentrations of several of the individual IHN and ICN, along with propanone nitrate during a major field campaign in Beijing as described in Sect. 3. In Sect. 4 we present the observed time series of the measured IN, examine their ratios and diel patterns. We a chemical box model to examine the ratio of the β-IHN isomers and how their ratio changes with NO, and to assess the key processes affecting the production and loss of all the IN measured (Sect. 5).

2 Nomenclature

In this paper when naming the IN we have followed the nomenclature described by Wennberg et al. (2018) . We assign numbers to the carbons of isoprene based on the conjugated butadiene backbone being comprised of carbons 1−4, with the methyl substituent (carbon 5) connected to carbon 2. We refer to these carbons as "C#" without subscripts (e.g., "C2"). For functionalized isoprene oxidation products, we drop the "C" when describing substituent positions; for example, (1-OH, 2-ONO_2)-isoprene hydroxy nitrate (IHN) has a hydroxy group at C1 and a nitrooxy group at C2. This is different to the way

we named the IN in Mills et al. (2016) in which the IHN naming followed that of Lockwood et al. (2010) and the ICN were named similarly to the equivalent IHN, except they have "–al" as a suffix. We referred to acetone nitrate as NOA in Mills et al. (2016) whereas here we refer to it as propanone nitrate.

3 Field campaigns and instrumentation

3.1 Field campaigns

The GC-NI-MS system was deployed in Beijing as part of the Atmospheric Pollution and Human Health in a Chinese Megacity (APHH-Beijing) programme (Shi et al., 2019) during two campaigns at the Institute of Atmospheric Physics (IAP), Chinese Academy of Sciences. IAP is located at 39.97° N, 116.38° E in a residential area between the 3rd and 4th North ring roads of Beijing. The site contained small trees and grass, with roads 150 m away. The first campaign was in winter (10th November to 10th December 2016) and the second in the summer (21st May to 22nd June 2017). For reasons discussed below we shall focus on the summer campaign.

Details of the isoprene nitrate measurement technique are provided below, whilst details of instrumentation used for the supporting data are provided in the Supp. Info.

3.2 Isoprene nitrate measurements

This was the first deployment of a GC-NI-MS system in the field to measure speciated isoprene nitrates. Measurements were made approximately hourly. Air was drawn at 10 L min^{-1} down a 2.5 m heated inlet (3/8" PFA and 45 °C) mounted on the roof (a height of approximately 3 m above the ground) of a mobile laboratory. During the summer campaign three different instrument setups were employed: (1) From the start of the measurements to 31 May, samples of 500 ml were taken off the inlet line down a 0.3 m length of 0.53 mm ID MxT-200 transfer line held at 50 °C and preconcentrated on a Tenax adsorption trap at 35 °C and 50 ml min^{-1}, and injected onto the column via a metal six port Valco valve by heating to 150 °C (Mills et al. 2016). A 30.5 m, 0.32 mm (internal diameter (ID)) combination column was used which was comprised of 28 m of Rtx-200 followed by 2.5 m of Rtx-1701 column. The GC oven was temperature profiled from 40 °C to 200 °C, with a constant column flow of 4.5 ml min^{-1} of helium; (2) Between 10th June and 16th June, the system was operated without a trap but instead direct injection of a 3 ml sample through a plastic Valco Cheminert valve connected to a short 0.32 mm ID

combination column (2.5 m of Rtx-200 joined to 0.5 m of Rtx-1701). The GC oven was temperature programmed from 10 °C to 200 °C and cooled with carbon dioxide (CO_2). A constant flow of 6.5 ml min^{-1} of helium was used as the carrier gas; (3) From 18th June to the end, the system again used the 30 m column and Tenax trapping as described above but the metal valve was replaced with the Cheminert valve that was used for the direct injections.

Of the compounds reported here, all but those of (1-OH, 2-ONO_2)-IHN and E-(1-ONO_2, 4-CO)-ICN were confirmed by injection of known isomers (Mills et al. 2016) post campaign. (1-OH, 2-ONO_2)-IHN was identified based on its expected elution just before (4-OH, 3-ONO_2)-IHN (Nguyen et al., 2014) and the similarity of the observed ions to those of (4-OH, 3-ONO_2)-IHN. The E-(1-ONO_2, 4-CO)-ICN peak was identified by its relative elution position compared to the other ICN (Schwantes et al., 2015), its expected retention time estimated from the relative retention times of known δ-IHN on this system and their aldehydic equivalents, and the similarity of observed ions to the other ICN.

During several comparisons of samples measured immediately before and after the valve was changed from metal to plastic and vice versa (1 h between samples), it was evident that the (4-OH, 3-ONO_2)-IHN and the ICN were lost to varying degrees on the metal valve as suggested by Crounse (J. D. Crounse, personal communication 2016), while simple alkyl nitrates were not. To account for this, all data obtained with the metal valve were scaled by the ratio of peak areas from the samples on either side of the valve changes to give results equivalent to those obtained when using the Cheminert valve.

Calibrations for (4-OH, 3-ONO_2)-IHN and propanone nitrate were derived from the relative sensitivity of the compound to that of n-butyl nitrate (Mills et al., 2016) corrected for the relative ion abundances of the specific measurement ions used for each compound (m/z 71 and 73, respectively). M/z 73 is a relatively minor ion for propanone nitrate, but we were unable to use a more major ion due to interferences from other compounds. N-butyl nitrate calibrations were performed every few days by attaching the transfer line to the standard in place of the inlet. We were unable to measure the relative sensitivities of (1-OH, 2-ONO_2)-IHN and the ICNs to n-butyl nitrate directly. To obtain an estimate, we have assumed that the ICN and propanone nitrate all have the same total ion yields compared to those of n-butyl nitrate and scaled this relative total ion yield by the fraction of the ion yield that the measurement ion represents. Similarly we have assumed that the total ion yields of (1-OH, 2-ONO_2)-IHN and (4-OH, 3-ONO_2)-IHN are the same (and thus the n-butyl nitrate m/z 71: total IN ion ratio) and scaled this to reflect the proportion of the total ions that m/z 101 represents for (1-OH, 2-ONO_2)-IHN.

3.3 Isoprene nitrate measurement uncertainties

We had previously determined the uncertainty for the measurement of the INs in laboratory (including the GCMS precision and calibration uncertainties) to be ±14 % (Mill et al, 2016), which includes an uncertainty of 5% for the GCMS precision. For determination of propanone nitrate in the field, we had to use a minor ion, and, with much smaller peaks, the precision

was worse than it had been in the laboratory using more abundant ions. Based on the signal to noise on a peak, we estimate that the precision was 10% rather than the 5%. We obtained ion counts per ppt of NO_Y for three isoprene nitrates: (4-OH, 3-ONO_2)-IHN (2030), propanone nitrate (2202) Z-(4-OH, 1-ONO_2)-IHN (2365). Using this range, we assume an additional uncertainty of 17% for the electron capture / ionisation efficiency of (1-OH, 2-ONO_2)-IHN and the ICN. During the campaign, we swapped between a metal and plastic valve twice. Using the peak areas for the last sample with the old valve and first sample with the new valve we calculated loss correction factors as well as the uncertainties in these correction factors of: (4-OH, 3-ONO_2)-IHN (±5.2%), propanone nitrate (±6.4%), E-(1-ONO_2, 4-CO)-ICN (±14.8%), E-(4-ONO_2, 1-CO)-ICN (±9.0%), Z-(1-ONO_2, 4-CO)-ICN (±7.5%) and Z-(4-ONO_2, 1-CO)-ICN (±9.2%). Loss corrections were applied to the data collected with the metal valve, and these additional uncertainties included in the overall uncertainties calculated for the periods when the metal valve was used. Based on Mills et al (2016) the detection limit (DL) of our system with the column and trap is 0.1 ppt, but this increased to 1 ppt when run with direct injection. Combining these uncertainties, we get overall uncertainties for the measurements of the IN as shown in Table 1.

When determining the uncertainties in the ratios between IN, we first calculated the uncertainties for each individual IN measurement excluding the calibration uncertainties that were common to both. We then combined the uncertainties in these to derive overall uncertainties in the ratios. We only assessed the ratios of 4-OH, 3-ONO_2)-IHN : (1-OH, 2-ONO_2)-IHN in period 2, when we the used the plastic valve and direct injection. I.e. for the ratio (4-OH, 3-ONO_2)-IHN : (1-OH, 2-ONO_2)-IHN, we considered the GCMS precision of 5% for each β-IHN and the additional 17% uncertainty for the electron capture / ionisation efficiency of (1-OH, 2-ONO_2)-IHN, plus the 1 ppt for the DL. We only assessed the ICN ratio in period 3 when we the used the plastic valve, along with column and trap. I.e. we considered the GCMS precision of 5% and the additional 17% uncertainty for the electron capture / ionisation efficiency for each of the ICN and 0.1 ppt for the DL.

4 Field observations

4.1 Overview of air quality conditions

During the winter campaign air quality was very poor with several haze events and average concentrations of $PM_{2.5}$ of ~90 μg m^{-3}, and average mixing ratios of NO_2 of 40 ppb, CO of 1300 ppb and O_3 of ~8 ppb (Shi et al., 2019). During the summer campaign air quality was also poor, but the mix of pollutants differed, with higher amounts of O_3 and lower amounts of $PM_{2.5}$, NO_2 and CO. i.e. average concentrations of $PM_{2.5}$ of ~30 μg m^{-3} and average mixing ratios of NO_2 of 15 ppb, CO of 450 ppb and O_3 of ~45 ppb (Shi et al., 2019).

4.2 Isoprene nitrate observations

4.2.1 Time series

The winter campaign was the first field deployment of the GC-NI-MS system for measuring isoprene nitrates. With the very poor air quality the air was loaded with nitrated species which led to many unidentifiable peaks in the chromatograms and, with low temperature and sunlight, biogenic emissions of isoprene were low and no IN were identified. We shall therefore limit our presentation of results to the summer campaign.

Seven individual isoprene nitrates were identified and quantified during the summer campaign (Fig. 1): two β-IHN ((1-OH, 2-ONO_2)-IHN, (4-OH, 3-ONO_2)-IHN); four ICN (E-(1-ONO_2, 4-CO)-ICN, Z-(1-ONO_2, 4-CO)-ICN, E-(4-ONO_2, 1-CO)-ICN, Z-(4-ONO_2, 1-CO)-ICN); and propanone nitrate.

Whilst we had previously demonstrated that the system can measure the four δ-IHN (Mills et al., 2016), we found no evidence of them in Beijing. This may not be so surprising given that Xiong et al. (2015) calculated the sum of the δ-IHN to have made up only a few percent of the total IHN during Southern Oxidant and Aerosol Study (SOAS) in the United States in 2013. Jenkin et al. (2015), using the Master Chemical Mechanism (MCMv3.3.1) (http:/mcm.york.ac.uk), calculated that the molar faction of IHN yield that would be made up of δ-IHN would increase with increasing NO such that for NO mixing ratios of 5-40 ppb typical of peak daytime values in Beijing this would be around 5-15% but less than 5% for mean daytime NO values of ~2.5 ppb. Note the isomer distribution will also be affected by loss processes and the δ-IHN have shorter lifetimes than the β-IHN (W2018).

The IN follow broadly similar temporal patterns with elevated mixing ratios for the first five days, followed by a period of five days of lower values before rising again (Fig. S1 in Supp. Info.). There were then breaks in data and a period of seven days whilst the GC-NI-MS was run in direct injection mode enabling the measurement of (1-OH, 2-ONO_2)-IHN along with (4-OH, 3-ONO_2)-IHN. During this period, these two β-IHN followed similar patterns (Fig. 2). There was then a final period when the trap was reinstalled when the other IN were measured again (Fig. S1).

The general trend in IN mixing ratios does not appear to be related to a similar trend in isoprene mixing ratios (Fig. S2). The isoprene time series exhibits a number of spikes in mixing ratios, several of which occurred at night. These are likely from very local sources, probably anthropogenic given the time of day, and injected into a shallow nocturnal mixed layer. The

highest mixing ratios of IN appear not to be related to polluted periods, but rather coincide with low NO mixing ratios when the NO_2:NO ratios were high (Figs. S1 and S2).

For the few days with measurements of both (1-OH, 2-ONO_2)-IHN and (4-OH, 3-ONO_2)-IHN available, the sum of the β-IHN show daily maxima of around 40-120 ppt with night-time values of around 10-30 ppt (Fig. 2). This is broadly similar to the sum of IHN reported for SOAS (Xiong et al., 2015; Schwantes et al., 2016). Likewise, our observed sum of the δ-ICN also exhibited night-time peaks of around 30-70 ppt (Figs. S1 and 3) which are broadly similar to those reported for SOAS (Schwantes et al., 2016). Our measurements of propanone nitrate often exceeded 50 ppt (Figs. S1 and 3) making them generally higher than those observed in SOAS, which rarely exceeded 40 ppt (Schwantes et al., 2016).

4.2.2 IN ratios

The two β-IHN are well correlated, with an R^2 value of 0.85. The mean for the ratio (1-OH, 2-ONO_2)-IHN : (4-OH, 3-ONO_2)-IHN is 3.4 (standard deviation of 1.7) and exhibits no clear diel cycle (Fig. 2). This compares with the average daytime ratios of ~2.6 and ~1.4 obtained by Vasquez et al. (2018) in Michigan during the PROPHET campaign and at Pasadena California, respectively. Xiong et al. (2015) calculate a ratio ranging from 2.6 to 6.0 based on the conditions experienced in SOAS. Jenkin et al. (2015), using the MCMv3.3.1, calculated that the ratio of (1-OH, 2-ONO_2)-IHN to (4-OH, 3-ONO_2)-IHN varies between about 1.5 and 2.5, decreasing with increasing NO and is around 2 for NO mixing ratios typical of the daytime values observed in Beijing (Fig. 4). It should be noted that the ratio we obtain from our measurements is not based on an independent calibration for (1-OH, 2-ONO_2)-IHN, but based on the assumption that the analytical system has the same sensitivity to (1-OH, 2-ONO_2)-IHN as it does to (4-OH, 3-ONO_2)-IHN. We have tried to account for this in the uncertainty calculations by assuming that the error in this sensitivity is equal to the percentage range of sensitivities that we observed for the other IN (see section 3.3). It is possible that this is an underestimate. The β-IHN ratio we obtain is broadly consistent with the studies described above and is examined in more detail with a model in Sect. 5.

Of the δ-ICN, the two *trans* (E) isomers have the highest mixing ratios with E-(1-ONO_2, 4-CO)-ICN being the most abundant (Fig. S1). Focusing on the last four days (three nights) of the summer campaign (Fig. 3), when we have most confidence in the data (i.e. when the plastic valve was used (Sect. 3.2)), we see that the observed ICN C1:C4 isomer ratio, exhibits a diel cycle with higher values at night (mean of 2.0, standard deviation (s.d.) of 0.3) and an overall mean of 1.4 (s.d. of 0.6). These values are considerably lower than would be expected based solely on the addition of NO_3 to isoprene occurring in the C1 and C4 positions in a ratio of 6 (C1:C4) (W2018). Our observed ratios are more comparable to the C1:C4 isomer ratio of 2.8 reported in Schwantes et al. (2016) for their environmental chamber. In their experiment the ICN mostly came from RO_2 + RO_2 reactions (see Sect. S1.2) because the NO and NO_3 concentrations were low. Although, we

had relatively higher NOx concentrations in Beijing, the afternoon mixing ratios of NO were often below 1 ppb (Fig. 4). Turning to the E:Z ratios, we observed the E-ICN isomers to dominate over the Z-ICN isomers. The (1-ONO_2, 4-CO)-ICN isomers exhibit a mean night-time E:Z ratio of 8 (s.d. of 1.4), whilst the (4-ONO_2, 1-CO)-ICN isomers exhibit a mean night-time E:Z ratio of 11 (s.d. of 1.5), giving an overall mean night-time E:Z ratio of 9 (s.d. of 1.0). These values are far greater than the *trans*:*cis* ratio of 1 presumed by W2018 for the reaction of NO_3 addition to isoprene, based on the OH addition to C1 of isoprene calculated by Peeters et al. (2009). However, it should be noted that the peroxy radicals formed from the reaction of the adducts with O_2 may be in a different ratio as these reactions are reversible, similar to those for peroxy radicals formed following OH addition to isoprene, as discussed in Sect. S1.1.

4.2.3 Diel patterns

In this section we examine the diel patterns of the IN and other trace gases by considering the means for each hour of the day (Fig. 4. Shaded areas represent ±1 s.d. in the variability of the measurements for each hour of the day). The isoprene mixing ratios exhibit a typical diel pattern with the highest values (~1 ppb) around midday, which are maintained through the afternoon before declining in the evening to near zero values at night. Much of the variability in the values, particularly at night, is caused by the high spikes shown in Fig. S1. O_3 mixing ratios build up gradually through the daytime, peaking mid to late afternoon and then slowly declining to minimum values around sunrise. Remarkably the mean diel peak value of O_3 was very high at around 100 ppb, demonstrating the considerable amount of photochemical pollution during the campaign. OH concentrations also exhibited a typical diel cycle peaking around midday at just below 1 x 10^7 molecules cm^{-3}. Evidence was found of low, but appreciable concentrations of OH at night, along with peroxy radicals, signifying the presence of nocturnal radical chemistry. NO peaked just after sunrise at around 7 ppb, and dropped below 1 ppb in the mid-afternoon.

The β-IHN, as illustrated by (4-OH, 3-ONO_2)-IHN, exhibit diel patterns (Fig. 4) that are consistent with formation from OH oxidation of isoprene (Sect.S1.2). They peak around midday and these levels are maintained until around sunset when they decline to reach minimum values just after sunrise. This pattern is broadly similar to that observed during SOAS for total IHN with a daytime peak of around 70 ppt and a minimum around sunset of around 10 ppt (Xiong et al., 2015). However, the SOAS IHN peaked earlier in the day at 10:00 Central Daylight Time, i.e. prior to the daytime maxima in OH and isoprene. Xiong et al. (2015) attribute this to competition between the different peroxy radical (ISOPOO) reactions, with the relative importance switching from reaction with NO to reaction with HO_2. Whilst NO mixing ratios peaked in the morning in Beijing, similar to those in SOAS, they are of greater magnitude and remain above 1 ppb until mid-afternoon (Fig. 4)), thus favouring IHN production for longer. Xiong et al. (2015) also suggest that mixing down of IHN from the residual layer may contribute to the morning increase in IHN mixing ratios. We will explore the diel pattern in (4-OH, 3-ONO_2)-IHN in more detail with a model in Sect. 5.

Conversely, the δ-ICN, as illustrated by E-(4-ONO_2, 1-CO)-ICN, exhibit nocturnal peaks, with maximum values in the early night and minimum values during the daytime (Fig. 4), which is consistent with formation from NO_3 addition to isoprene (Sect. S1.2) in the evening and a lifetime of the order of a few hours or less. The mean mixing ratio increases in the evening at a rate of 3 ppt h^{-1} from around 2 to 8 ppt in 2 hours. We calculated the concentrations of NO_3 required to produce such an increase by considering its loss via reactions with OH, O_3 and NO_3, and its production from NO_3 addition to isoprene with an assumed yield of ~5 %. We use bimolecular rate coefficients given in W2018 and number densities of the reactants from the observations (Fig. 4). This calculation assumes that the rate limiting step in the production of (4-ONO_2, 1-CO)-ICN is the reaction of isoprene with NO_3 and that deposition is negligible. The 5 % yield is based on Schwantes et al. (2015) chamber experiments results, whereby we assume a 20 % yield of ICN from NO_3 addition to isoprene, of which 25 % is E-(4-ONO_2, 1-CO)-ICN. We calculate that ~3 ppt of NO_3 is required to produce the observed evening increase in E-(4-ONO_2, 1-CO)-ICN, which is consistent with the observed NO_3 mixing ratios (mean values rise from 2 ppt to 8 ppt from 18:00 to 20:00) (Fig. 4).

Interestingly, ~1-2 ppt of E-(4-ONO_2, 1-CO)-ICN persists during the daytime. We performed a similar calculation to the above, but this time assuming steady state and a photolysis rate based on Xiong et al. (2016) (i.e. a value of 4.6×10^{-4} s^{-1} for a solar zenith angle of 0° and adjusting for latitude, time of year and time of day). We find that around 1-2 ppt of NO_3 is required to produce the observed E-(4-ONO_2, 1-CO)-ICN. Whilst we observe this amount during the afternoon, mean values in the morning are ~0.2-0.5 ppt (Fig. 4). This might suggest mixing down of ICN into the mixed layer in the morning but would require considerable production of ICN in the residual layer during the previous evening/night.

As noted above, the ratios of C1-ICN to C4-ICN ratios exhibit diel patterns (Fig. 3). The ratios are higher at night and lower in the daytime. The evening ratios are driven by the preferential addition of NO_3 to the C1 position as discussed above in Sect. 4.2.2. The decrease in this ratio during the morning could be explained if the lifetime of C1-ICN were shorter than for the other isomers. However, the rate coefficients for reaction with OH recommended by W2018 are about 20 % slower for C1-ICN than for C4-ICN. Photolysis is expected to be the largest daytime sink, but Xiong et al (2016) only determined this for E-(4-ONO_2, 1-CO)-ICN. There is a hint of a diel pattern in the ratio of the E and Z isomers of (1-ONO_2, 4-CO)-ICN, with larger values at night, but during the daytime the Z isomers are at or below our detection limit of 0.1 ppt leading to large uncertainties in the calculated ratios.

Propanone nitrate shows no clear diel cycle. The pattern can change from day to day, sometimes peaking during the daytime and sometimes at night-time. This is illustrated in Fig. 3 which shows the temporal variation of propanone nitrate, along with (4-OH, 3-ONO_2)-IHN and (4-ONO_2, 1-CO)-ICN for the last four days of the campaign. Propanone nitrate peaks on the night of the 19/06/2017 coincident with the ICN. This is followed by two peaks, one in the night of the 20-21/06/2017, again

coincident with the ICN, and then a second peak during the daytime of the 21/06/2017 when (4-OH, 3-ONO_2)-IHN maximises. Schwantes et al. (2016) noted that on some days during the SOAS campaign propanone nitrate increased after sunrise following the presence of ICN the night before, while on other occasions night-time ICN was not followed by increases in propanone nitrate, or propanone nitrate appeared during the day when ICN had not been present the night before. They suggest that as well as photooxidation of the ICN, boundary layer dynamics may have played a role as propanone nitrate may have been formed aloft in a residual layer at night and was then mixed down to the surface in the morning. We investigate the night-time and daytime sources of propanone nitrate during the Beijing campaign further in Sect. 5.5 using a model.

5 MCM Box modelling

5.1 MCM model set up

A zero dimensional box model, utilising a subset of the chemistry described within the Master Chemical Mechanism, MCMv3.3.1 (Jenkin et al., 2015), was used to calculate the concentration of the various isoprene nitrates for comparison with those measured. The MCMv3.3.1 includes an update of the isoprene degradation chemistry to reflect findings of recent laboratory and theoretical studies.

The model was constrained by measured values of water vapour, temperature, pressure, NO, NO_2, NO_3, O_3, CO, SO_2, HONO and HCHO. Speciated VOC measurements of alcohols, alkanes, alkenes, dialkenes (including isoprene), multi-functional aromatics, carbonyls and monoterpenes were included as further model constraints. The concentrations of H_2 and CH_4 were held constant at 500 ppb and 1.8 ppm, respectively. The photolysis rates for j(O^1D), j(NO_2) and j(HONO), calculated from the measured actinic flux and published absorption cross sections and quantum yields, were included as model inputs. Other photolysis frequencies used in the model were calculated. For UV-active species, such as HCHO and CH_3CHO, photolysis rates were calculated by scaling to the ratio of clear-sky j(O^1D) to observed j(O^1D) to account for clouds. For species able to photolyse further into the visible the ratio of clear-sky j(NO_2) to observed j(NO_2) was used. The variation of the clear-sky photolysis rates (j) with solar zenith angle (χ) was calculated within the model using the following expression:

$$j = l\cos(\chi)^m \times e^{-n\sec(\chi)} \quad (3)$$

with the parameters *l*, *m* and *n* optimised for each photolysis frequency (see Table 2 in Saunders et al. (2003)).

The model was run for the entirety of the campaign (21st May 2017 – 25th June 2017) in overlapping 7 day segments, with the model constraints updated every 15 minutes. By this method, a model time-series was produced which could be directly compared with observations and, from which, diel averages were generated. There was a spike of very high concentrations of isoprene in the early hours of the morning of 16th June 2017, which led to extremely high concentrations of modelled ICN, propanone nitrate and (4-OH, 1-ONO_2)-IHN. These have been removed from the diel averages presented in this paper. Fluxes through each reaction were calculated for every 15 minute period to allow an analysis of the production and loss terms of the chemical species.

The loss due to mixing of all non-constrained, model generated species, including the speciated isoprene nitrates, was parametrised and evaluated by comparing the model-predicted glyoxal concentration with the observed glyoxal concentration. Applying a loss rate proportional to the observationally-derived mixed layer height (Fig. 4), the model was able to reproduce glyoxal observations reasonably well. As a result of this first order loss process, the partial lifetime of the model generated species was ~2 h at night, then decreased rapidly to a lifetime of <30 min in the morning as the mixed layer grew, effectively simulating ventilation of the model box. With the collapse of the mixed layer in the late afternoon the model lifetime with respect to ventilation of glyoxal (and other model generated species) increased. However, the model has a tendency to underestimate glyoxal concentrations between 4 pm and midnight. This underestimation suggests that either the lifetime with respect to ventilation should be even longer or that the model is underestimating oxidation processes that lead to glyoxal production at these times.

5.2 β-IHN

Figs. S3 and 5 compare the measured and modelled β-IHN. The shaded areas in Fig. 5 represent ±1 s.d. in the data for each hour of the day and illustrate the large day-to-day variability in the mixing ratios of β -IHN. Note that for (1-OH, 2-ONO_2)-IHN there are only 6 days of data, hence why the average diel patterns are strongly affected by the day-to-day variability. This is particularly the case for the measurements where three of the hourly bins contain just one measurement, and the rest have between three and eight measurements.

The MCM simulates (1-OH, 2-ONO_2)-IHN daytime mixing ratios very similar to those observed. The modelled evening mixing ratios are lower than observed. Like glyoxal, this underestimation suggests the lifetime with respect to ventilation might be longer than 2 hours.

During the daytime the (4-OH, 3-ONO_2)-IHN modelled by the MCM tends to give larger mean mixing ratios and greater day-to-day variability than observed. This is partially the result of a few days when the model calculates high mixing ratios of (4-OH, 3-ONO_2)-IHN that are not observed (Fig. S3). Like the modelled (1-OH, 2-ONO_2)-IHN, the concentrations of (4-OH, 3-ONO_2)-IHN decline more rapidly in the evening than observed, suggesting that its lifetime with respect to ventilation might be longer than 2 hours.

To limit the impact of mixing on the comparison between the model and observations, Figs. 2 and 6 compare the ratios of (1-OH, 2-ONO_2)-IHN to (4-OH, 3-ONO_2)-IHN. When looking at the times series (Fig. 2) of this ratio the model and measurements often agree within the measurement uncertainties, although there are times when the modelled values are less that observed. The shaded areas in Fig. 6 represent ±1 s.d. in the data for each hour of the day. The large variability in the observed data are caused by some hours having very few data points, sometimes affected by a single high value (Fig. 2). The MCM simulates mean ratios that, are generally lower than the observed mean, although they are sometimes within the uncertainty of the measured ratio and often within the day-to-day variability.

There are four main factors that determine the ratio of the β-IHN: 1) the yields of their respective peroxy radicals (ISOPOO) following oxidation of isoprene by OH addition (φ); 2) the fraction of the respective ISOPOO that reacts with NO (γ); 3) the branching ratios for the formation of the IHN from the reaction of NO with the ISOPOO (α); and 4) the relative loss rates of the β-IHN, including via deposition.

For the first two factors, the concentration of NO is largely the determining influence. NO is often present in large amounts (Figs 4 and S2) so that reaction with it is the dominant loss process for the ISOPOO. NO is the major factor determining the lifetime of the ISOPOO and therefore the extent of the redistribution of the ISOPOO from a kinetic ratio towards a thermodynamic equilibrium. The adducts formed from OH addition to a specific C in isoprene can form a β-ISOPOO and either a *trans* or *cis* δ-ISOPOO. These reactions are reversible and occur at different rates which along with the rapid 1,6 H atom shift isomerisation of the Z-δ-ISOPOO means that the longer the lifetime of the ISOPOO the more the ratio of the β-ISOPOO shifts towards (1-OH, 2-OO)-ISOPOO. Consequently, at lower NO mixing ratios the ratio of φ-(1-OH, 2-ONO_2)-IHN to φ-(4-OH, 3-ONO_2)-IHN becomes larger. This is illustrated in Fig. 7a, which shows the modelled ratio of the values of φ. For mixing ratios of NO greater than ~2 ppb the ratio of the values of φ decreases approximately linearly from around 2 to about 1.7 at 100 ppb of NO. The ratio of the kinetic yields in the MCM is 1.58, which is the ratio of the values of φ that we get if we switch off the reverse pathway of the O_2 reactions. This implies that even at 100 ppb of NO, the ratio of the yields of the (1-OH, 2-OO)-ISOPOO to (4-OH, 3-OO)-ISOPOO is shifted to values slightly greater than the kinetic ratio. At NO mixing ratios less than ~2 ppb the ratio of the values of φ increase greatly with decreasing NO, such that at a few 10s of ppt of NO the ratio is typically between 2.5 and 4.

The rates at which the ISOPOO are assumed to be lost via the reactions with NO, HO_2 and NO_3 are the same for both β-ISOPOO. However, the rate of reaction for (1-OH, 2-OO)-ISOPOO with RO_2 and its rate of isomerisation are slower than for (4-OH, 3-OO)-ISOPOO. At lower NO mixing ratios, these reactions become relatively more important and so the value of γ is lower for (4-OH, 3-OO)-ISOPOO than for (1-OH, 2-OO)-ISOPOO, therefore the ratio of γ-(1-OH, 2-OO)-ISOPOO to γ-(4-OH, 3-OO)-ISOPOO is larger (Fig. 7b). This is further enhanced as the concentrations of RO_2 can also be much greater at the lower NO concentrations, particularly below 1 ppb of NO (Fig. 7c), which leads to the ratio in the γ values being considerably greater than 1 at NO concentrations below a few 10s of ppt.

It should be noted that the MCM model underestimates the measured RO_2 mixing ratios. This will lead to underestimation of the ratio of γ-(1-OH, 2-OO)-ISOPOO to γ-(4-OH, 3-OO)-ISOPOO, primarily at mixing ratios of NO below ~2 ppb. This might explain some of the differences between the MCM modelled and observed β-IHN ratios.

The net effect of these relationships is that the ratio of (1-OH, 2-OO)-ISOPOO to (4-OH, 3-OO)-ISOPOO increases with decreasing NO (Fig. 7d), i.e. for NO mixing ratios greater than 2 ppb the ratio is around 1.7-2.0, but at NO mixing ratios less than 2 ppb the ratio increases up towards a value of around 4. The ratio of the rate of production of (1-OH, 2-ONO_2)-IHN to (4-OH, 3-ONO_2)-IHN will have the same relationship with NO as the ratio of their precursor ISOPOO since the MCM assumes that the branching ratios for the formation of the two β-IHN from the reaction of NO with the ISOPOO (i.e. α, third factor) are the same. However, there are still considerable uncertainties in these branching ratios (Sect. S1.1).

As for the loss processes of the β-IHN (fourth factor), the dominant loss in the model is the mixing term which is set at the same rate for both β-IHN. Photolysis is assumed to be faster for (1-OH, 2-ONO_2)-IHN than for (4-OH, 3-ONO_2)-IHN in the MCM, but is only a minor loss process. However, (1-OH, 2-ONO_2)-IHN reacts with both OH and O_3 more slowly than does (4-OH, 3-ONO_2)-IHN and since the dominant chemical loss process for the β-IHN are by far their reactions with OH, the net effect of these loss processes is to increase the ratio of (1-OH, 2-ONO_2)-IHN to (4-OH, 3-ONO_2)-IHN above their production ratio. The diel pattern in OH (Fig. 4) will tend to increase the ratio of 1-OH, 2-ONO_2)-IHN to (4-OH, 3-ONO_2)-IHN during the daytime.

Regarding deposition, it is not included in the MCM model. We expect (1-OH, 2-ONO_2)-IHN to be lost more efficiently than (4-OH, 3-ONO_2)-IHN given the fast rate of hydrolysis reported for (1-OH, 2-ONO_2)-IHN (W2018) (Sect. S1.3.5) and the greater difficulty we have getting (1-OH, 2-ONO_2)-IHN through our analytical system indicating a greater loss of this isomer on to surfaces. However, including a greater deposition rate for (1-OH, 2-ONO_2)-IHN would reduce the agreement with the observed β-IHN ratios.

Overall, this means that the modelled ratio of (1-OH, 2-ONO_2)-IHN to (4-OH, 3-ONO_2)-IHN increases with decreasing NO mixing ratios (Fig. 7e) (as also seen by Jenkin et al. (2015) in a box model using the MCM), and generally does not drop below the ratio of the β-ISOPOO (Fig. 7d). In the conditions modelled for Beijing, at NO mixing ratios above ~30 ppb it remains between 1.75 and 2.0. At NO mixing ratios between 1 ppb and ~30 ppb it is mostly around 2.0 but is sometimes up to 3. At NO mixing ratios below 1 ppb, it is typically between 2 and 3, but sometimes up to 4. There are several cases at these low NO mixing ratios when the ratio of the β-IHN is below the ratio of the β-ISOPOO, but these occur at night when the production rates and the mixing ratios of the β-IHN are very small.

Newland et al., (2020) point out that during the campaign a high NO_X environment existed in the morning that then switched to a low NO_X environment in the afternoon. The mean hourly NO mixing ratios were typically above 2 ppb between 06:00 and 12:00 local time, but mostly below this value in the afternoon (Fig. 4) when production rates of the β-IHN were also high. This largely explains why the modelled ratio of the β-IHN (Fig. 6), is ~2 between about 06:00 and 09:00 and then rises up to around 2.5 in the afternoon. The modelled variability in this ratio is very small between 06:00 and 09:00 as the ratio of 2 relates to a wide range of NO mixing ratios (~2-30 ppb) (Fig. 7e).

In comparison, the observed ratios of (1-OH, 2-ONO_2)-IHN to (4-OH, 3-ONO_2)-IHN show a much weaker relationship with NO (Fig. 7f). This may be due to there being far fewer data points and uncertainties in the measurements. The observed ratios tend to be higher than modelled. At times they drop below the kinetic ratio for φ (but with the uncertainty range of the measurements). Despite far more scatter, including 2 outliers with large uncertainties, there is a tendency for higher values of the observed ratio at NO mixing ratios of less than 1 ppb, as simulated by the model.

Vasquez et al. (2018) reported lower daytime values for the ratio of (1-OH, 2-ONO_2)-IHN to (4-OH, 3-ONO_2)-IHN in PROPHET campaign (~2.6) and in Pasadena (~1.4) compared to our observations of ~3.4, but their data show a similar pattern to ours in that the ratio is higher in the low NO_X environment of PROPHET compared to the high NO_X environment in Pasadena. On average our modelled results are close to the ratios observed in PROPHET. We cannot rule out calibration differences affecting this comparison and like us Vasquez et al (2018) relied on relative calibrations estimates. Also, differences in the observed β-IHN ratios may be due to the amount and reactivity of the peroxy radicals present in the different studies. However, the ratio of 1.4 observed for Pasadena is lower than the value of around 1.75 that we calculate for NO mixing ratios of 100 ppb, and furthermore, it is also lower than the kinetic φ ratios of 1.58 and 1.85 based on MCM and W2018 kinetic yields, respectively.

5.3 δ-ICN

The δ-ICN time series (Fig. S4) shows that the MCM often produces far more δ-ICN than observed, particularly at night. This is further illustrated by the diel patterns (Fig. 8), which shows both higher modelled mixing ratios and greater day-to-day variability at night compared to the observations. Moreover, the model simulates an increase in the daytime δ-ICN that far exceeds that seen in the observations. We are unable to assess the ratios of the different δ-ICN isomers using the model as the MCM assumes all of the δ-ICN formed can be represented by a single species, (1-ONO_2, 4-CO)-ICN, called NC4CHO in the MCM.

The source of δ-ICN is via the addition of NO_3 to isoprene followed by addition of O_2. This produces δ-nitroxy peroxy radicals (INO_2) (NISOPO2 in the MCM) and, in the conditions simulated for Beijing, the major loss of NISOPO2 is reaction with NO to form NO_2 and a δ-nitroxy alkoxy radical (NISOPO in the MCM), which then reacts rapidly with O_2 to form the δ-ICN (NC4CHO). Other production pathways for NC4CHO exist in the MCM, but the reaction of NISOPO with NO is by far the dominant source of δ-ICN in our simulations. There are some nights when there are large sources of NISOPO2, but typically the production of NISOPO2 maximises in the mid-afternoon when isoprene concentrations are still high and mean NO_3 mixing ratios were observed to be around 2 ppt (Fig. 4). Consequently, the production of δ-ICN in the model is mostly during the daytime, despite NO_3 usually being considered to be more important at night. Comparison of the modelled and observed mixing ratios of the δ-ICNs suggest that this source might be too fast even during the daytime, despite the model being constrained by observed concentrations of isoprene and NO_3.

Alternatively, the loss processes could be too slow. The dominant loss in the model is the mixing term, which is greatest during the daytime when the mixed layer is fully developed. The same loss process has been applied to all model generated species (Sect. 5.1). For glyoxal, (1-OH, 2-ONO_2)-IHN and (4-OH, 3-ONO_2)-IHN, the model tends to overestimate the decrease in concentrations from late afternoon onwards suggesting that the lifetime with respect to mixing should be longer at these times. Increasing the lifetime of all the model intermediates would lead to a further overestimation of δ-ICN. Applying the same loss term to all model species is of course an approximation, not least because the dilution term depends on the concentration of the species in the diluent air.

The next most important loss processes for δ-ICN are simulated to be photolysis and reaction with OH, which are also both predominantly daytime losses. The net effect of the production and loss terms is that the modelled δ-ICN maximise during the night-time as obsdeved (Fig. 8).

The MCM uses a photolysis frequency for δ-ICN based on that measured for propanone nitrate, which is equivalent to 3.16 x 10^{-4} s^{-1} for a solar zenith angle of 0°. Xiong et al. (2016) determined a rate of 4.6 x 10^{-4} s^{-1} for (4-ONO_2, 1-CO)-ICN for a solar zenith angle of 0°. Reaction with OH constitutes a similar size loss for δ-ICN as photolysis in the model. Whilst these are both predominantly daytime sinks, increasing them would not only reduce the daytime increase in δ-ICN but would also

reduce the amount of modelled δ-ICN that would persist into the night. The MCM treats all the δ-ICN as (1-ONO_2, 4-CO,)-ICN and uses a rate coefficient for reaction with OH of 4.1 x 10^{-11} cm^3 s^{-1}. However, W2018 suggests a lower rate coefficient for reaction of OH with (4-ONO_2, 1-CO)-ICN than for (1-ONO_2, 4-CO,)-ICN (3.4 x 10^{-11} cm^3 s^{-1} versus 4.1 x 10^{-11} cm^3 s^{-1}). Therefore, treating the two separately in the model would, overall, reduce the loss of δ-ICN with respect to OH, increasing discrepancy with the model.

Night-time losses of δ-ICN are reaction with O_3 and NO_3. The MCM uses a rate coefficient of 2.4 x 10^{-17} cm^3 s^{-1} for the reaction of δ-ICN with O_3, which is 5 times faster than the rate of 4.4 x 10^{-18} cm^3 s^{-1} recommended by W2018, giving a partial lifetime on the order of 12 hours for an O_3 mixing ratio of 40 ppb. On the other hand, the MCM uses a rate for the reaction of δ-ICN with NO_3 which is 10 times slower than the rate recommended by W2018, but even so the lifetime of δ-ICN with respect to reaction with NO_3 as estimated by W2018 is of the order of 4 days, so this loss pathway would have to be much faster to reduce the modelled night-time δ-ICN to close to that observed.

5.4 Propanone nitrate

Figures S4 and 8 show the time series and diel patterns of the measured and modelled propanone nitrate. The observed mixing ratios are generally higher than the modelled values. As discussed above, elevated propanone nitrate mixing ratios are observed both during the daytime and night-time, leading to a weak bimodal pattern in the mean, but there is large day-to-day variability. This is consistent with both daytime and night-time production processes. It should be noted that transport will play an important role in the variability of the propanone nitrate. Its chemical lifetime is calculated to be around 10 hours during the daytime and considerably longer at night. The mixing term dominates the modelled lifetime so the resulting mixing ratios are highly dependent on the assumptions regarding this term. However, the model can still provide insight into the dominant chemical processes.

The main source of propanone nitrate is via oxidation of isoprene, with routes via both OH and NO_3 addition to isoprene. Its primary source in the MCM simulation is via the OH oxidation of NC4CHO (i.e. the δ-ICN) and this is reflected in them sharing many similarities in their modelled time series (Fig S4). As discussed in Sect. 5.3, the production of NC4CHO and its loss via OH oxidation occur mostly during the daytime, so this source of propanone nitrate is predominantly during the daytime. On nights when OH is present even at low concentrations it can be a sizeable source due to the relatively large amounts of NC4CHO at night. Propanone nitrate is also formed from oxidation of NC4CHO by O_3. This is a relatively small source except on nights when O_3 was present (Fig. S2).

The modelled ratio propanone nitrate to δ-ICN is mostly much less than one. Conversely the measured propanone nitrate is typically a lot greater than the total δ-ICN observed. This might, in part be due to the model being unable to simulate the mixing correctly, but, as discussed in Sect. 5.3, the model simulates considerably larger amounts of NC4CHO than observed and getting the wrong balance between the various production and loss terms of NC4CHO (i.e. the δ-ICN) will likely impact the modelled propanone nitrate.

Propanone nitrate can also be produced following the NO_3 addition to propene. Overall, the model results suggest this to be a relatively small source, but at night it is often calculated to be the dominant source, which may explain some of the night-time peaks in propanone nitrate.

5.5 δ-IHN

The MCM simulates daytime peak mixing ratios for the δ-IHN (i.e. (1-OH, 4-ONO_2)-IHN and (4-OH, 1-ONO_2)-IHN), consistent with production from OH addition to isoprene, of around 1 ppt (Figs. 9 and S5). As mentioned above, we were unable to detect these IN in Beijing despite having been able to in the laboratory. The two δ-IHN are simulated to have very similar mixing ratios during the daytime, but on several nights, enhancements of (4-OH, 1-ONO_2)-IHN are simulated and these are coincident with enhanced modelled mixing ratios of the δ-ICN. As well as being formed by OH oxidation of isoprene, (4-OH, 1-ONO_2)-IHN is also formed in the MCM when the NISOPO2 radicals produced by NO_3 oxidation of isoprene react with other organic peroxy radicals. As discussed above in Sect. 5.3, NISOPO2 are mostly present during the daytime, but on some nights NISOPO2 mixing ratios were simulated to be high leading to elevated mixing ratios of both (4-OH, 1-ONO_2)-IHN and δ-ICN. Only a few of the simulated night-time peaks occurred at times when we were making measurements, but despite the modelled mixing ratios of around 15-30 ppt being well above our detection limit we did not to detect (4-OH, 1-ONO_2)-IHN. Also, despite successfully measuring the δ-ICN, we did not detect strong enhancements in their mixing ratios.

6 Conclusions

Examining the ratio of the two β-IHN in a box model demonstrates its sensitivity to NO, which affects the thermodynamic equilibrium of the β-ISOPOO and the competition between the reactions of the β-ISOPOO with NO and with RO_2. In both cases, lower NO mixing ratios favour (1-OH, 2-ONO_2)-IHN over (4-OH, 3-ONO_2)-IHN. Interestingly, in high NO_X conditions the modelled β-IHN ratio ((1-OH, 2-OO)-ISOPOO to (4-OH, 3-OO)-ISOPOO) of around 2 exceeds the kinetic

ratio. At NO mixing ratios below 2 ppb the competition between the reactions of the β-ISOPOO with NO and with RO_2 become important and this results in modelled β-IHN ratios greater than 2, approaching 4 for NO mixing ratios of a few 10s of ppt.

The observed mean β-IHN ratio is 3.4, higher than modelled. The relationship of the observed β-IHN ratio with NO is much weaker than modelled, partly due to far fewer data points, but it confirms the theoretical understanding in so far as there tend to be larger ratios at sub 2 ppb amounts of NO.

The diel variation in NO mixing ratios means that the NO_X environment observed in Beijing typically switched from a high NO_X environment in the morning to a low NO_X environment in the afternoon resulting in a diel pattern of the modelled β-IHN ratio. However, this is not reflected in the observations, largely due to lack of measurements and the day-to-day variability seen on the few days of available data. More observations of speciated β-IHN and a more accurate calibration of (1-OH, 2-ONO_2)-IHN are needed to better constrain these relationships and the underlying chemistry.

Of the δ-ICN, the two *trans* isomers are observed to have the highest mixing ratios, with E-(1-ONO_2, 4-CO)-ICN being the most abundant. However, the mean C1:C4 isomer ratio is 1.4, which is considerably lower than would be expected based solely on the addition of NO_3 to isoprene occurring in the C1 and C4 positions in a 6:1 ratio. This raises the question as to whether it is appropriate to represent the δ-ICN by a single C1 nitrated isomer, as done in the MCM. We observed the *trans*-ICN isomers to dominate over the *cis*-ICN isomers with a mean ratio of 7 far greater than the *trans*:*cis* ratio of 1 presumed by W2018 for the reaction of NO_3 addition to isoprene. This suggests that thermodynamic redistribution of the nitrated peroxy radicals formed from the reaction of the NO_3-isoprene adducts with O_2 may also be important.

The observed δ-ICN exhibit nocturnal peaks with maximum values in the early night and minimum values during the daytime are consistent with formation from NO_3 addition to isoprene in the evening and a lifetime of the order of a few hours or less. Mixing ratios of 1-2 ppt persist through the daytime, which for the afternoon can be accounted for by the presence of 1-2 ppt of NO_3. The model produces far more δ-ICN than observed, particularly at night but it also simulates an increase in the daytime δ-ICN that greatly exceeds that seen in the observations. Reaction of NO with NISOPO2, which comes from NO_3 addition to isoprene, is modelled to be by the far the dominant source of δ-ICN. Interestingly, though this source occurs predominantly during the daytime, due to the presence in Beijing of appreciable daytime amounts of NO_3 along with isoprene.

Observed propanone nitrate shows no clear diel cycle. The pattern can change from day to day, sometimes peaking during the daytime and sometimes at night. The model suggests that the main source of propanone nitrate is the daytime OH oxidation of δ-ICN. However, the model simulates considerably larger amounts of δ-ICN than observed and getting the right

balance between the various production and loss terms of δ-ICN is important for modelling the propanone nitrate. Whilst the model results suggest the NO_3 addition to propene to be a relatively small source of propanone nitrate, at night it is often calculated to be the dominant source, which may explain some of the night-time peaks in propanone nitrate.

The main source of the δ-IHN is modelled to come from OH addition to isoprene, but on certain nights the source from NO_3 addition to isoprene led to modelled mixing ratios of around 15-30 ppt of (4-OH, 1-ONO_2)-IHN coincident with enhanced modelled mixing ratios of the δ-ICN. We were unable to detect δ-IHN despite the modelled mixing ratios being considerably greater than our detection limit, nor did we detect strong enhancements in the mixing ratios of the δ-ICN, so again raises questions concerning our understanding of the NO_3 initiated isoprene degradation chemistry

This study demonstrates the need for further measurements of speciated IN measurements to test our understanding of the isoprene degradation chemistry. Our interpretation is limited by the uncertainties in our measurements and relatively small data set, but highlights areas of the isoprene chemistry that warrant further study, in particular the impact of NO on the formation of the β-IHN, and the NO_3 initiated isoprene degradation chemistry.

Code Availability. The MCM code is available from the authors on request.

Data Availability. The observational data and diel cycles from the MCM in the figures are in the Supplementary Information. The 15 minute data from the MCM is available from the authors on request.

Supplement.

Author contributions. CER led the data interpretation and writing of the manuscript. GPM made the measurements of the IN with the assistance of YL. LKW did the MCM modelling. CER, WJB, SG, DEH, CNH, RLJ, JDL, XW and CY were involved in the project planning and leading the measurement groups. WJA, LRC, JRH, SK, LJK, BO, ES, FS and RW-M provided measurement data. All commented on the manuscript.

Competing interests. The authors declare that they have no conflict of interest.

Acknowledgements. We are grateful for funding provided by the UK Natural Environment Research Council (NERC), UK Medical Research Council and the Natural Science Foundation of China (NSFC) under the framework of the Newton Innovation Fund (NERC grants NE/N006909/1, NE/N006895/1, NE/N006976/1 and NE/N00700X/1; NSFC grant 41571130031). ES and RW-M are grateful to the NERC SPHERES Doctoral Training Programme for funding PhD studentships. CER acknowledges Andrew Rickard (NCAS, University of York) for providing information on the MCM.

References

Bates, K. H., and Jacob, D. J., A new model mechanism for atmospheric oxidation of isoprene: global effects on oxidants, nitrogen oxides, organic products, and secondary organic aerosol, Atmos. Chem. Phys., 19, 9613–9640, https://doi.org/10.5194/acp-19-9613-2019, 2019.

Beaver, M. R., St Clair, J. M., Paulot, F., Spencer, K. M., Crounse, J. D., LaFranchi, B. W., Min, K. E., Pusede, S. E., Wooldridge, P. J., Schade, G. W., Park, C., Cohen, R. C., and Wennberg, P. O.: Importance of biogenic precursors to the budget of organic nitrates: observations of multifunctional organic nitrates by CIMS and TD-LIF during BEARPEX 2009, Atmos. Chem. Phys., 12, 5773-5785, doi: 10.5194/acp-12-5773-2012, 2012.

Bew, S. P., Hiatt-Gipson, G. D., Mills, G. P., and Reeves, C. E.: Efficient syntheses of climate impacting isoprene nitrates and (1R,5S)-(-)-myrtenol nitrate, Beilstein J. Org. Chem., 12, 1081–1095, doi:10.3762/bjoc.12.103, 2016.

Bohn, B., Heard, D. E., Mihalopoulos, N., Plass-Dülmer, C., Schmitt, R., and Whalley, L. K.: Characterisation and improvement of $j(O^1D)$ filter radiometers, Atmos. Meas. Tech., 9, 3455– 3466, https://doi.org/10.5194/amt-9-3455-2016, 2016.

Brown, S. S., de Gouw, J. A. Warneke, C., Ryerson, T. B., Dubé, W. P., Atlas, E., Weber, R. J., Reltier, R. E., Neuman, J. A., Roberts, J. M., Swanson, A., Flocke, F., McKeen, S. A., Brioude, J., Sommariva, R., Trainer, Fehsenfeld, F. C., and Ravishankara, A. R.: Nocturnal isoprene oxidation over the Northeast United States in summer and its impact on reactive nitrogen partitioning and secondary organic aerosol, Atmos. Chem. Phys., 9, 3027-3042, 2009.

Chen, X., Hulbert, D., and Shepson, P. B.: Measurement of the organic nitrate yield from OH reaction with isoprene, J. Geophys. Res., 103, 25,563-25,568, 1998.

Chuong, B., and Stevens, P. S.: Measurements of the Kinetics of the OH-Initiated Oxidation of Isoprene. J. Geophys. Res., 107 (D13), ACH 2-1−ACH 2-12, 2002.

Crilley, L. R., Kramer, L., Pope, F. D., Whalley, L. K., Cryer, D. R., Heard, D. E., Lee, J. D., Reed, C., and Bloss, W. J.: On the interpretation of in situ HONO observations via photochemical steady state., Faraday. Discuss., 189, 191–212, 2016.

Cryer (2016): Measurements of hydroxyl radical reactivity and formaldehyde in the Atmosphere, PhD Thesis University of Leeds.

Emmerson, K. M., and Evans, M. J.: Comparison of tropospheric gas-phase chemistry schemes for use within global models, Atmos. Chem. Phys., 9, 1831-1845, 2009.

Fiore, A. M., Horowitz, L. W., Purves, D. W., Levy II, H., Evans, M. J., Wang, Y., Li, Q., and Yantosca, R. M.: Evaluating the contribution of changes in isoprene emissions to surface ozone trends over the eastern United States, J. Geophys. Res., 110, D12303, doi: 10.1029/2004JD005485, 2005.

Fisher, J. A., Jacob, D. J., Travis, K. R., Kim, P. S., Marais, E. A., Chan Miller, C., Yu, K., Zhu, L., Yantosca, R. M., Sulprizio, M. P., Mao J., Wennberg, P. O., Crounse, J. D., Teng, A. P., Nguyen, T. B., St. Clair, J. M., Cohen, R. C., Romer, P., Nault, B. A., Wooldridge, P. J., Jimenez, J. L., Campuzano-Jost, P., Day, D. A., Hu, W., Shepson, P. B., Xiong, F., Blake, D. R., Goldstein, A. H., Misztal, P. K., Hanisco, T. H., Wolfe, G. M., Ryerson, T. B., Wisthaler, A., and Mikoviny, T.: Organic Nitrate Chemistry and its Implications for Nitrogen Budgets in an Isoprene- and Monoterpene-Rich Atmosphere: Constraints from Aircraft (SEAC^{4}RS) and Ground-Based (SOAS) Observations in the Southeast US. Atmos. Chem. Phys. 16, 5969−5991, 2016.

Giacopelli, P., Ford, K., Espada, C., and Shepson, P. B.: Comparison of the measured and simulated isoprene nitrate distributions above a forest canopy, J. Geophys. Res., 110, D01304, doi:10.1029/2004JD005123, 2005.

Grossenbacher, J. W., Couch, T., Shepson, P. B., Thornberry, T., Witmer-Rich, M., Carroll, M. A., Faloona, I., Tan, D., Brune, W., Ostling, K., and Bertman, S.: Measurements of isoprene nitrates above a forest canopy, J. Geophys. Res., 106, 24429–24438, 2001.

Grossenbacher, J. W., Barlet Jr., D. J., Shepson, P. B., Carroll, M. A., Olszyna, K., and Apel, E.: A comparison of isoprene nitrate concentrations at two forest-impacted sites, J. Geophys. Res., 109, D11, D11311, doi: 10.1029/2003JD003966, 2004.

Guenther, A., Jiang, X., Heald, C. L., Sakulyanontvittaya, T., Duhl, T., Emmons, L. K., and Wang, X.: The Model of Emissions of Gases and Aerosols from Nature version 2.1 (MEGAN 2.1): An Extended and Updated Framework for Modeling Biogenic Emissions. Geosci. Model Dev., 5, 1471−1492, 2012.

Horowitz, L. W., Fiore, G. P., Milly, A. M., Cohen, R. C., Perring, A., Wooldridge, P. J., Hess, P. G., Emmons, L. K., and Lamarque, J.: Observational constraints on the chemistry of isoprene nitrates over the eastern United States, J. Geophys. Res., 112, D12S08, doi:10.1029/2006JD007747, 2007.

Jacobs, M. I., Burke, W. J., and Elrod, M. J.: Kinetics of the reactions of isoprene-derived hydroxynitrates: gas phase epoxide formation and solution phase hydrolysis, Atmos. Chem. Phys., 14, 8933-8946, doi: 10.5194/acp-14-8933-2014, 2014.

Jenkin, M. E., Young, J. C., and Rickard, A. R.: The MCM v3.3.1 degradation scheme for isoprene, Atmos. Chem. Phys., 15, 11433-11459, doi: 10.5194/acp-15-11433-2015, 2015.

Kennedy, O. J., Ouyang, B., Langridge, J. M., Daniels, M. J. S., Bauguitte, S., Freshwater, R., McLeod, M. W., Ironmonger, C., Sendall, J., Norris, O., Nightingale, R., Ball, S. M., and Jones, R. L.: An aircraft based three channel broadband cavity enhanced absorption spectrometer for simultaneous measurements of NO_3, N_2O_5 and NO_2, Atmos. Meas. Tech., 4, 9, 1759-1776, DOI: 10.5194/amt-4-1759-2011, 2011.

Kotthaus, S. and Grimmond, C. S. B.: Atmospheric boundary layer characteristics from ceilometer measurements part 1: A new method to track mixed layer height and classify clouds, Q. J. Roy. Meteorol. Soc., 144, 1525–1538, https://doi.org/10.1002/qj.3299, 2018.

Kwan, A. J., Chan, A. W. H., Ng, N. L., Kjaergaard, H. G., Seinfeld, J. H., and Wennberg, P. O.: Peroxy Radical Chemistry and OH Radical Production during the NO3-Initiated Oxidation of Isoprene, Atmos. Chem. Phys., 12, 7499−7515, 2012.

Lee, L., Teng, A. P., Wennberg, P. O., Crounse, J. D., and Cohen, R. C.: On Rates and Mechanisms of OH and O_3 Reactions with Isoprene Derived Hydroxy Nitrates, J. Phys. Chem., 118, 1622-1637, doi: 10.1021/jp4107603, 2014.

Lee, B. H., Lopez-Hilfiker, F. D., D'Ambro, E. L., Zhou, P., Boy, M., Petäjä, T., Hao, L., Virtanen, A., and Thornton, J. A.: Semi-volatile and highly oxygenated gaseous and particulate organic compounds observed above a boreal forest canopy, Atmos. Chem. Phys., 18, 11547-11562, doi: 10.5194/acp-18-11547-2018, 2018.

Li, R., Jiang, X., Wang, X., Chen, T., Du, L., Xue, L., Bi, X,. Tang, M., and Wang, W., Determination of Semivolatile Organic Nitrates in Ambient Atmosphere by Gas Chromatography/Electron Ionization–Mass Spectrometry, Atmosphere, 10, 88, doi:10.3390/atmos10020088, 2019.

Lockwood, A. L., Shepson, P. B., Fiddler, M. N., and Alaghmand, M.: Isoprene nitrates: preparation, separation, identification, yields, and atmospheric chemistry, Atmos. Chem. Phys., 10, 6169-6178, doi: 10.5194/acp-10-6169-2010, 2010.

Mao, J., Paulot, F., Jacob, D. J., Cohen, R. C., Crounse, J. D., Wennberg, P. O., Keller, C. A., Hudman, R. C., Barkley, M. P., and Horowitz, L. W.: Ozone and organic nitrates over the eastern United States: Sensitivity to isoprene chemistry, J. Geophys. Res.: Atmospheres, 118, 11,256-11,268, doi: 10.1002/jgrd.50817, 2013.

Mills, G. P., Hiatt-Gipson, G. D., Bew, S. P., and Reeves, C. E.: Measurement of isoprene nitrates by GCMS, Atmos. Meas. Tech., 9, 4533-4545, doi: 10.5194/amt-9-4533-2016, 2016.

Müller, J.-F., Peeters, J., and Stavrakou, T.: Fast photolysis of carbonyl nitrates from isoprene, Atmos. Chem. Phys., 14, 2497-2508, doi: 10.5194/acp-14-2497-2014, 2014.

Newland, M. J., Bryant, D. J., Dunmore, R. E., Bannan, T. J., Acton, W. J. F., Langford, B., Hopkins, J. R., Squires, F. A., Dixon, W., Drysdale, W. S., Ivatt, P. D., Evans, M. J., Edwards, P. M., Whalley, L. K., Heard, D. E., Slater, E. J., Woodward-Massey, R., Ye, C., Mehra, A., Worrall, S. D., Bacak, A., Coe, H., Percival, C. J., Hewitt. C. N., Lee, J. D., Cui, T., Surratt, J. D., Wang, X., Lewis, A. C., Rickard. A. R., Hamilton, J. F., Rainforest-like Atmospheric Chemistry in a Polluted Megacity, Atmos. Chem, Phys., under review, https://doi.org/10.5194/acp-2020-35, 2020.

Nguyen, T. B., Crounse, J. D., Schwantes, R. H., Teng, A. P., Bates, K. H., Zhang, X., St. Clair, J. M., Brune, W. H., Tyndall, G. S., Keutsch, F. N., Seinfeld, J. H., and Wennberg, P. O.: Overview of the Focused Isoprene eXperiment at the

California Institute of Technology (FIXCIT): mechanistic chamber studies on the oxidation of biogenic compounds, Atmos. Chem. Phys., 14, 13531-13549, doi: 10.5194/acp-14-13531-2014, 2014.

Nguyen, T. B., Crounse, J. D., Teng, A. P., St Clair, J. M., Paulot, F., Wolfe, G. M., and Wennberg, P. O.: Rapid deposition of oxidized biogenic compounds to a temperate forest, P. Natl. Acad. Sci., 112, E392-E401, doi: 10.1073/pnas.1418702112, 2015.

Paulot, F., Crounse, J. D., Kjaergaard, H. G., Kroll, J. H., Seinfeld, J. H., and Wennberg, P. O.: Isoprene photooxidation: new insights into the production of acids and organic nitrates, Atmos. Chem. Phys., 9, 1479-1501, 2009.

Paulot, F., Henze, D. K., and Wennberg, P. O.: Impact of the isoprene photochemical cascade on tropical ozone, Atmos. Chem. Phys., 12, 1307-1325, doi: 10.5194/acp-12-1307-2012, 2012.

Peeters, J., Nguyen, T. L., and Vereecken, L.: HOx radical regeneration in the oxidation of isoprene, Phys. Chem. Chem. Phys., 28, 5935–5939, 2009.

Perring, A.E., Bertram, T.H., Wooldridge, P.J., Fried, A., Heikes, B.G., Dibb, J., Crounse, J.D., Wennberg, P.O., Blake, N.J., Blake, D.R., Brune, W.H., Singh, H.B., and Cohen, R.C, Airborne observations of total $RONO_2$: new constraints on the yield and lifetime of isoprene nitrates., Atmos. Chem. Phys., 9 (4), 1451-1463, 2009a.

Perring, A. E., Wisthaler, A., Graus, M., Wooldridge, P. J., Lockwood, A. L., Mielke, L. H., Shepson, P. B., Hansel, A., and Cohen, R. C., A product study of the isoprene+NO_3 reaction, Atmos. Chem. Phys., 9(14), 4945-4956, 2009b.

Rollins, A. W., Kiendler-Scharr, A., Fry, J. L., Brauers, T., Brown, S. S., Dorn, H.-P., Dubé, W. P., Fuchs, H., Mensah, A., Mentel, T. F., Rohrer, F., Tillmann, R., Wegener, R., Wooldridge, P. J., and Cohen, R. C.: Isoprene oxidation by nitrate radical: alkyl nitrate and secondary organic aerosol yields, Atmos. Chem. Phys., 9, 6685-6703, 2009.

Saunders, S. M., Jenkin, M. E., Derwent, R. G., and Pilling, M. J.: Protocol for the development of the Master Chemical Mechanism, MCM v3 (Part A): tropospheric degradation of non-aromatic volatile organic compounds, Atmos. Chem. Phys., 3, 161-180, 2003.

Schwantes, R. H., Teng, A. P., Nguyen, T. B., Coggon, M. M., Crounse, J. D., St Clair, J. M., Zhang, X., Schilling, K. A., Seinfeld, J. H. and Wennberg, P. O.: Isoprene NO_3 Oxidation Products from the RO_2 + HO_2 Pathway, J. Phys. Chem., 119, 10158-10171, doi: 10.1021/acs.jpca.5b06355, 2015.

Schwantes, R. H., Emmons, L. K., Orlando, J. J., Barth, M. C., Tyndall, G. S., Hall, S. R., Ullmann, K., St. Clair, J. M., Blake, D. R., Wisthaler, A., and Bui, T. P. V., Comprehensive isoprene and terpene gas-phase chemistry improves simulated surface ozone in the southeastern US, Atmos. Chem. Phys., 20, 3739–3776, https://doi.org/10.5194/acp-20-3739-2020, 2020.

Shi, Z., Vu, T., Kotthaus, S., Harrison, R. M., Grimmond, S., Yue, S., Zhu,T., Lee,J., Han,Y., Demuzere,M., Dunmore,R.E., Ren, L., Liu,D., Wang,Y., Wild,O., Allan,J., Acton,W.J., Barlow,J., Barratt, B., Beddows, D., Bloss, W. J., Calzolai, G.,

Carruthers, D., Carslaw, D. C., Chan, Q., Chatzidiakou, L., Chen, Y., Crilley, L., Coe, H., Dai, T., Doherty, R., Duan, F., Fu, P., Ge, B., Ge, M., Guan, D., Hamilton, J. F., He, K., Heal, M., Heard, D., Hewitt, C. N., Hollaway, M., Hu, M., Ji, D., Jiang, X., Jones, R., Kalberer, M., Kelly, F. J., Kramer, L., Langford, B., Lin, C., Lewis, A. C., Li, J., Li, W., Liu, H., Liu, J., Loh, M., Lu, K., Lucarelli, F., Mann, G., McFiggans, G., Miller, M. R., Mills, G., Monk, P., Nemitz, E., O'Connor, F., Ouyang, B., Palmer, P. I., Percival, C., Popoola, O., Reeves, C., Rickard, A. R., Shao, L., Shi, G., Spracklen, D., Stevenson, D., Sun, Y., Sun, Z., Tao, S., Tong, S., Wang, Q., Wang, W., Wang, X., Wang, X., Wang, Z., Wei, L., Whalley, L., Wu, X., Wu, Z., Xie, P., Yang, F., Zhang, Q.,Zhang, Y.,Zhang,Y., and Zheng, M.: Introduction to the special issue "In-depth study of air pollution sources and processes within Beijing and its surrounding region (APHH-Beijing)", Atmos. Chem. Phys., 19, 7519–7546, https://doi.org/10.5194/acp19-7519-2019, 2019.

Smith, K. R., Edwards, P. M., Evans, M. J., Lee, J. D., Shaw, M. D., Squires, F., Wilde, S., and Lewis, A. C.: Clustering approaches to improve the performance of low cost air pollution sensors, Faraday Discuss., 200, 321–637, https://doi.org/10.1039/C7FD00020K, 2017.

Squire, O. J., Archibald, A. T., Griffiths, P. T., Jenkin, M. E., Smith, D., and Pyle, J. A: Influence of isoprene chemical mechanism on modelled changes in tropospheric ozone due to climate and land use over the 21st century, Atmos. Chem. Phys., 15, 5123-5143, doi: 10.5194/acp-15-5123-2015, 2015.

Teng, A. P., Crounse, J. D., and Wennberg, P. O.: Isoprene Peroxy Radical Dynamics, J. Am. Che. Soc., 139, 5367-5377, doi: 10.121/jacs.6b12838, 2017.

Vasquez, K. T., Allen, H. M., Crounse, J. D., Praske, E., Xu, L., Noelscher, A. C., and Wennberg, P. O.: Low-pressure gas chromatography with chemical ionization mass spectrometry for quantification of multifunctional organic compounds in the atmosphere, Atmos. Meas. Tech., 11, 6815-6832, doi: 10.5194/amt-11-6815-2018, 2018.

Von Kuhlmann, R., Lawrence, M. G., Pöschl, U., and Crutzen, P. J.: Sensitivities in global scale modeling of isoprene, Atmos. Chem. Phys., 4, 1-17, 2004.

Werner, G., Kastler, J ., Looser, R., and Ballschmiter, K., Organic nitrates of isoprene as atmospheric trace compounds, Angewandte Chemie-Int. Ed., 38(11), 1634-1637. 1999. DOI: 10.1002/(SICI)1521-3773(19990601)38:11

Wennberg, P. O., Bates, K. H., Crounse, J. D., Dodson, L. G., McVay, R. C., Mertens, L. A., Nguyen, T. B., Praske, E., Schwantes, R. H., Smarte, M. D., St Clair, J. M., Teng, A. P., Zhang, X., and Seinfeld, J. H.: Gas-Phase Reactions of Isoprene and Its Major Oxidation Products, Chem. Rev., 118, 3337-3390, doi: 10.1021/acs.chemrev.7b00439, 2018.

Wu, S., Mickley, L. J., Jacob, D. J., Logan, J. A. Yantosca, R. M., and Rind, D.: Why are there large differences between models in global budgets of tropospheric ozone?, J. Geophys. Res., 112, D5, D05302, doi: 10.1029/2006JD007801, 2007.

Xie, Y., Paulot, F., Carter, W. P. L., Nolte, C. G., Luecken, D. J., Hutzell, W. T., Wennberg, P. O., Cohen, R. C., and Pinder, R. W.: Understanding the impact of recent advances in isoprene photooxidation on simulations of regional air quality, Atmos. Chem. Phys., 13, 8439-8455, doi: doi:10.5194/acp-13-8439-2013, 2013.

Xiong, F., McAvey, K. M., Pratt, K. A., Groff, C. J., Hostetler, M. A., Lipton, M. A., Starn, T. K., Seeley, J. V., Bertman, S. B., Teng, A. P., Crounse, J. D., Nguyen, T. B., Wennberg, P. O., Misztal, P. K., Goldstein, A. H., Guenther, A. B., Koss, A. R., Olson,K. F., de Gouw, J. A., Baumann, K., Edgerton, E. S., Feiner, P. A., Zhang, L., Miller, D. O., Brune, W. H., and Shepson, P. B.: Observation of isoprene hydroxynitrates in the southeastern United States and implications for the fate of NOx, Atmos. Chem. Phys., 15, 11257-11272, doi: 10.5194/acp-15-11257-2015, 2015.

Xiong, F., Borca, C. H., Slipchenko, L. V., and Shepson, P. B.: Photochemical degradation of isoprene-derived 4,1-nitrooxy enal, Atmos. Chem. Phys., 16, 5595-5610, doi: 10.5194/acp-16-5595-2016, 2016.

Zare, A., Romer, P. S., Nguyen, T., Keutsch, F. N., Skog, K., and Cohen, R. C.: A comprehensive organic nitrate chemistry: insights into the life time of atmospheric organic nitrates, Atmos. Chem. Phys., 15, 15419-15436, doi: 10.5194/acp-18-15419-2018, 2018.

Table 1: Uncertainties in the measurements of the isoprene nitrates

Isoprene nitrate	Period 1 (metal valve, column and trap)	Period 2 (plastic valve and direct injection)	Period 3 (plastic valve, column and trap)
(4-OH, 3-ONO_2)-IHN	15% + 0.1 ppt	14% + 1 ppt	14% +0.1 ppt
(1-OH, 2-ONO_2)-IHN	-	22% + 1 ppt	-
E-(1-OH, 4-ONO_2)-ICN	27% + 0.1 ppt	-	22% +0.1 ppt
E-(4-OH, 1-ONO_2)-ICN	24% + 0.1 ppt	-	22% +0.1 ppt
Z-(1-OH, 4-ONO_2)-ICN	23% + 0.1 ppt	-	22% +0.1 ppt
Z-(4-OH, 1-ONO_2)-ICN	24% + 0.1 ppt	-	22% +0.1 ppt
Propanone nitrate	18% + 0.1 ppt	-	17% +0.1 ppt

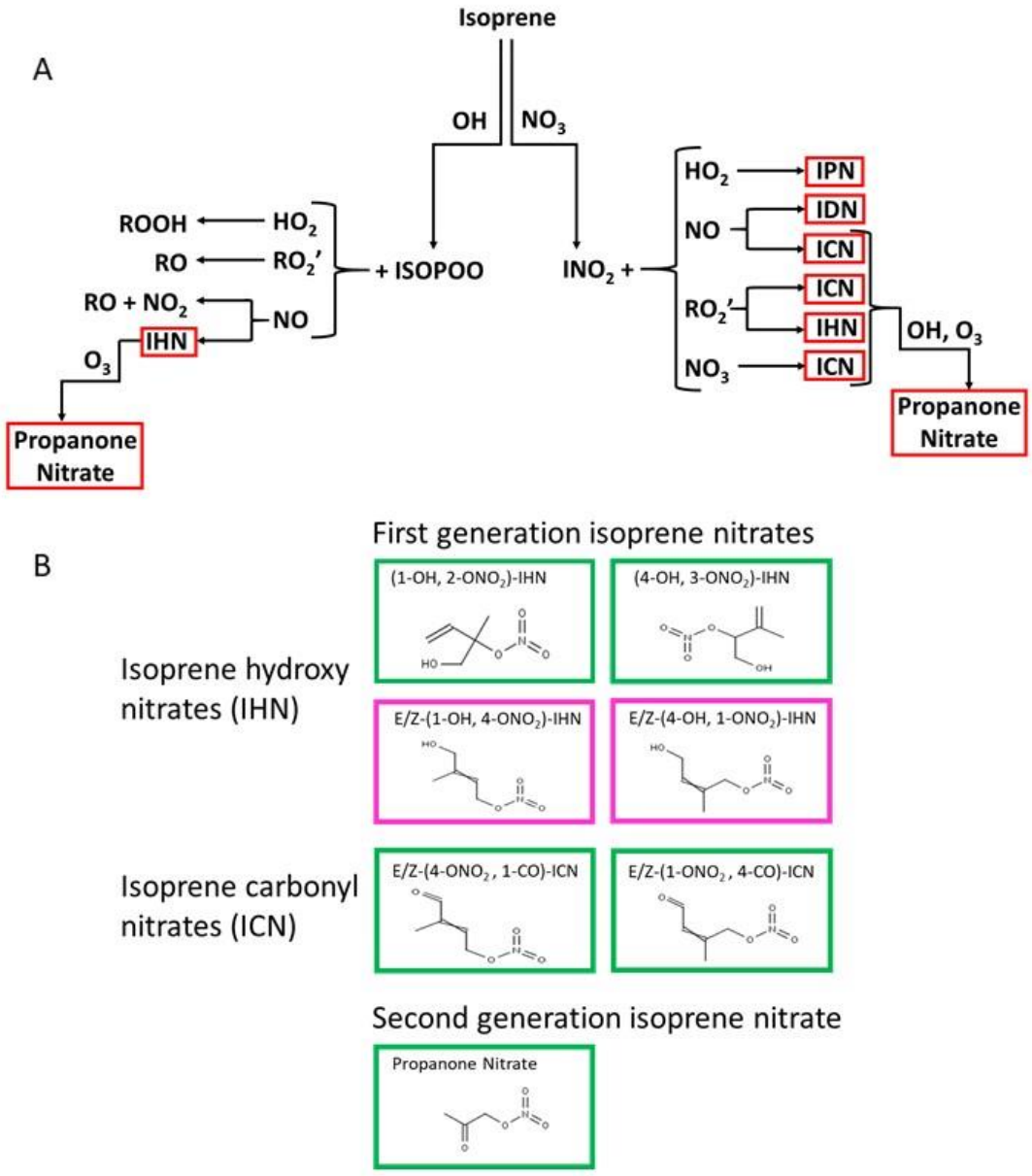

855 **Figure 1: A) Formation of IN (red boxes) from isoprene oxidation by OH and NO_3: isoprene hydroxy nitrates (IHN): isoprene hydroperoxy nitrates (IPN); isoprene dinitrates (IDN); isoprene carbonyl nitrates (ICN); and propanone nitrate. B) The skeletal formula of the specific IN discussed in this paper. Box colours: Green - measured in Beijing; Pink - measured by the analytical system previously in the laboratory, but not discernible in Beijing.**

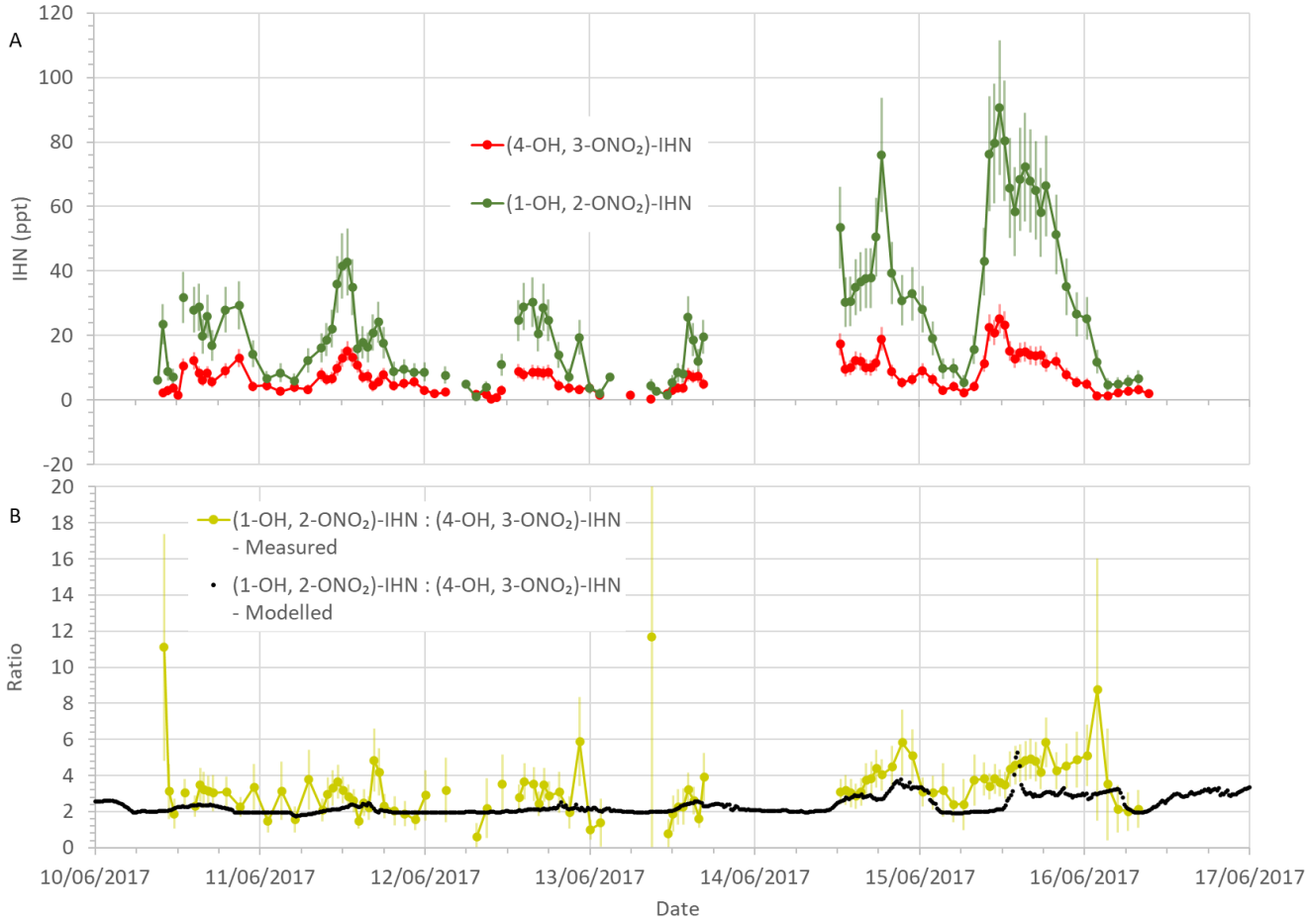

Figure 2: a) Measured β-IHN mixing ratios. b) Measured and modelled ratio (1-OH, 2-ONO_2)-IHN:(4-OH, 3-ONO_2)-IHN. Error bars are the measurement uncertainties (see Sect. 3.3 for details).

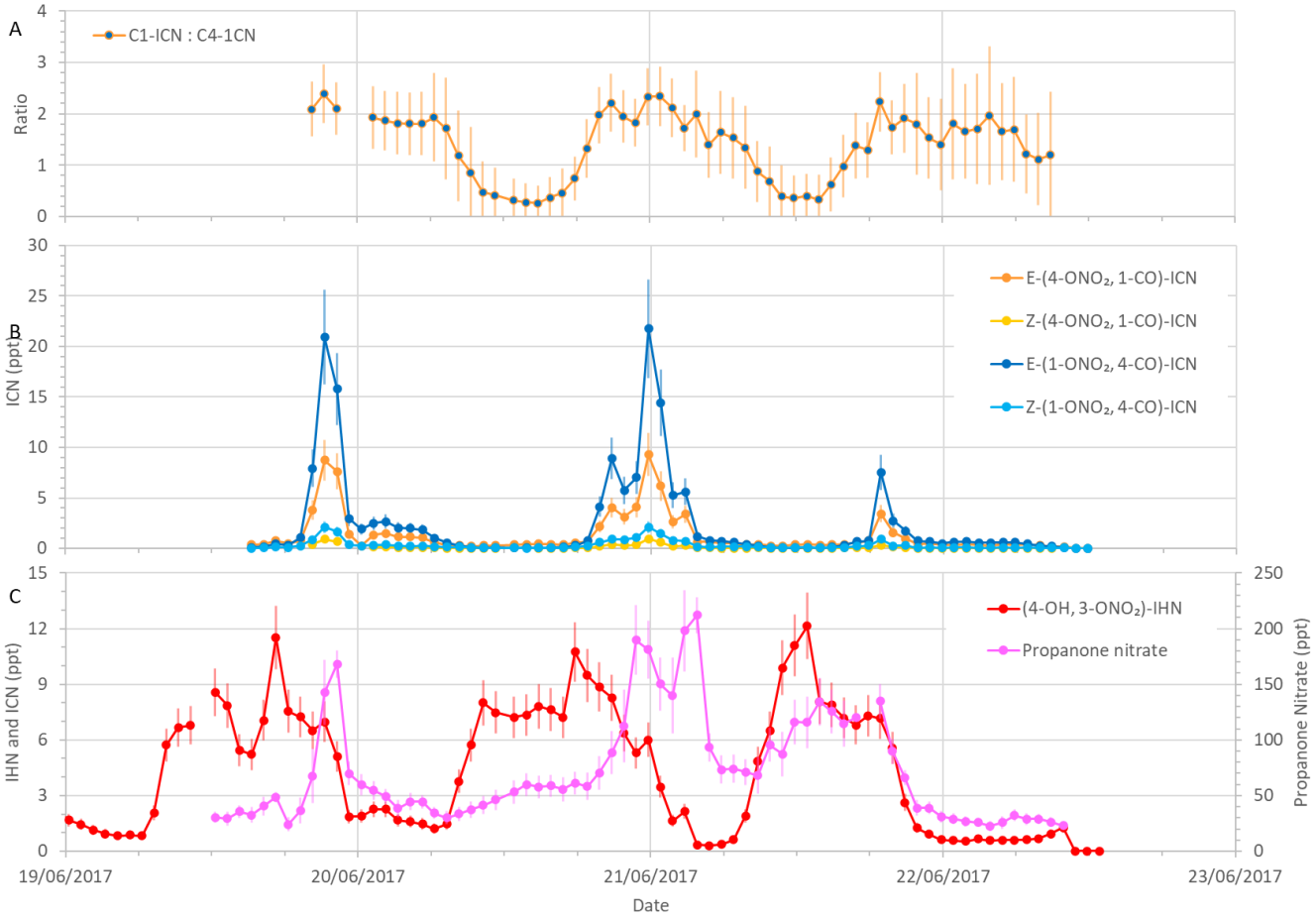

Figure 3: Measured δ-ICN mixing ratios and ratios of C1-ICN to C4-ICN, along with (4-OH, 3-ONO$_2$)-IHN and propanone nitrate mixing ratios during the last four days of the summer campaign. Error bars are the measurement uncertainties (see Sect. 3.3 for details).

870

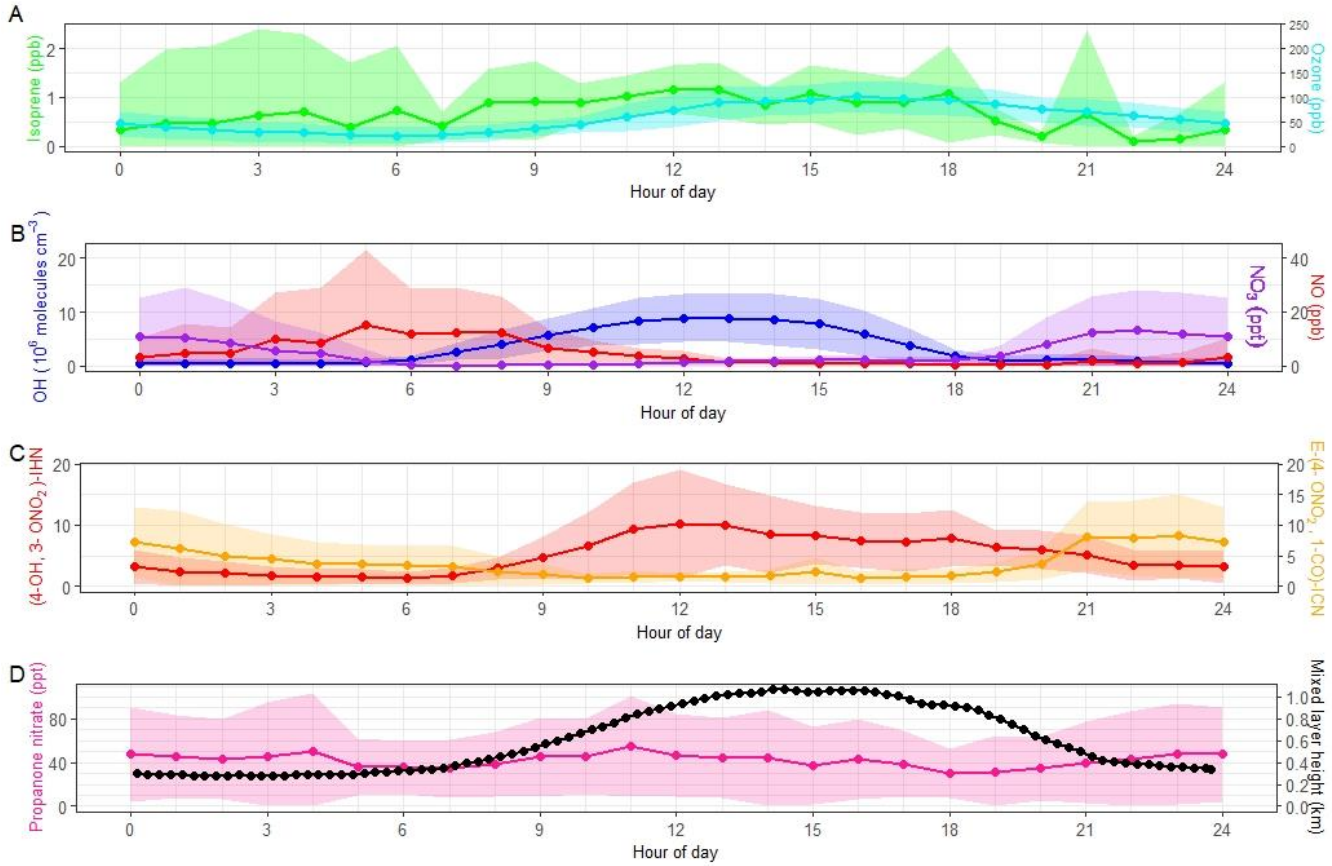

Figure 4: Diel patterns of trace gases derived from the measured mixing ratios for each hour of the day. Data points for the mixing ratios are the means and the shaded areas represent ±1 s.d. in the variability of values for each hour of the day. Also shown are the means of the mixed layer height for each 15 minute period of the day.

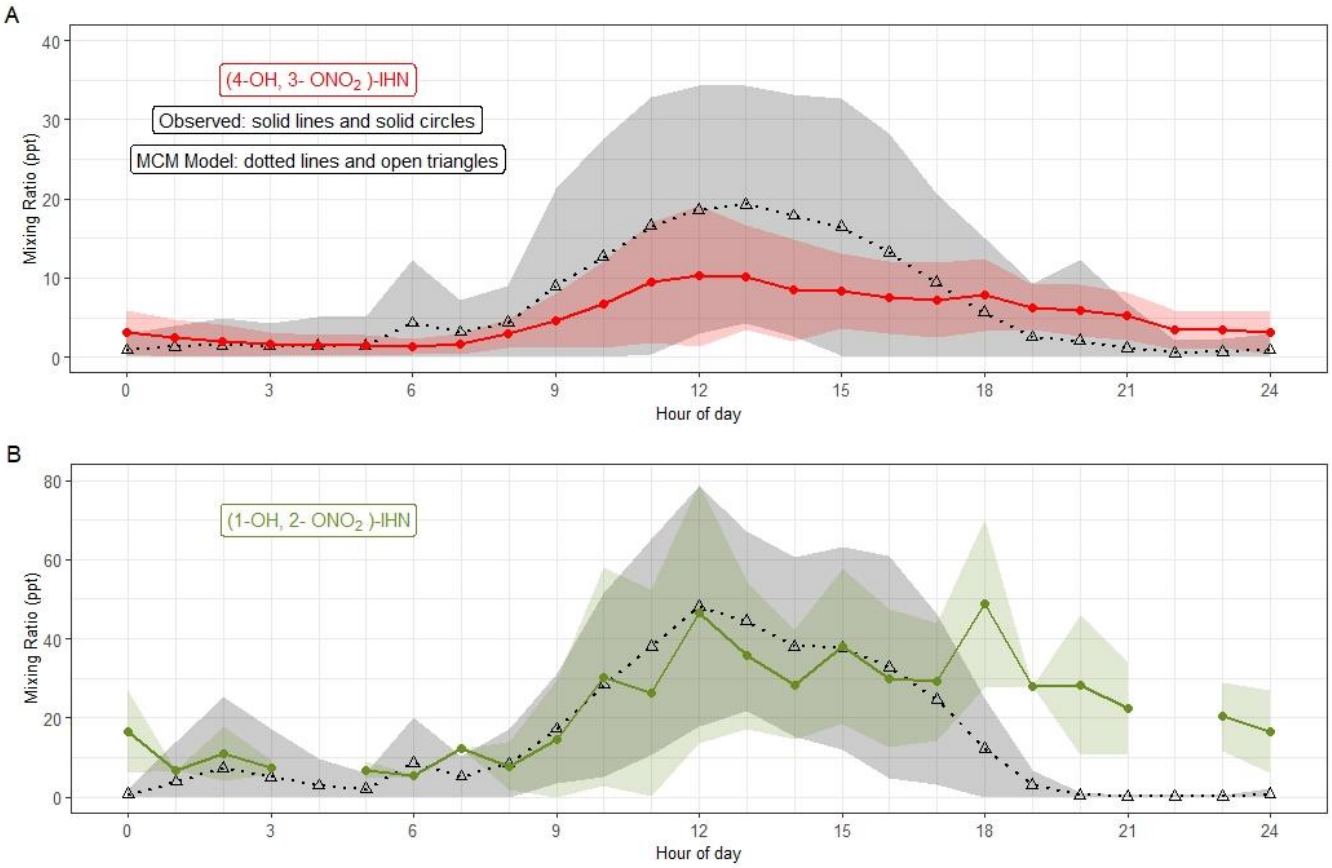

Figure 5: Modelled and observed mixing ratios of (a) (4-OH, 3-ONO_2)-IHN and (b) (1-OH, 2-ONO_2)-IHN. Data points are the means and the shaded areas represent ±1 s.d. in the variability of values for each hour of the day.

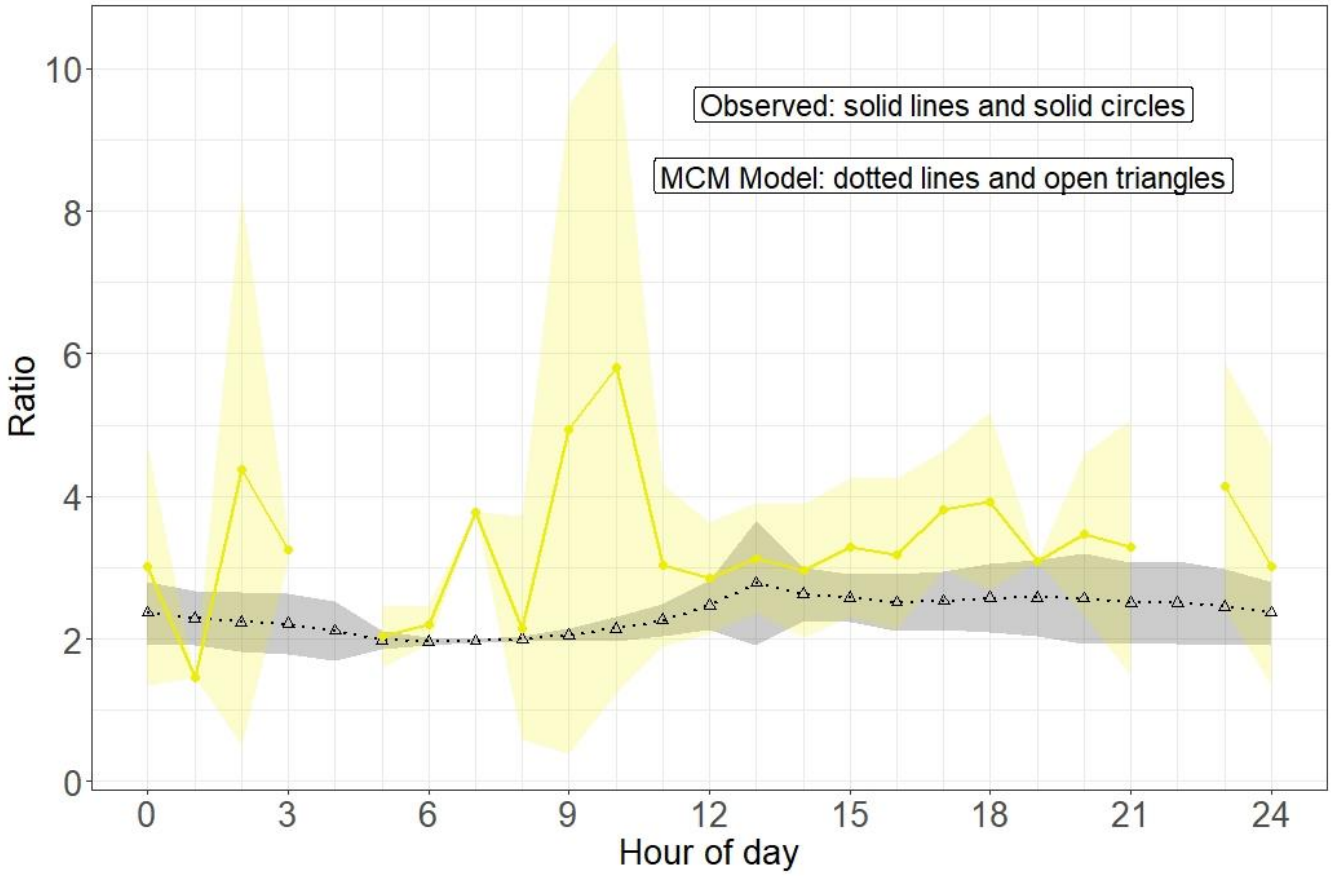

Figure 6: Modelled and observed (1-OH, 2-ONO_2)-IHN / (4-OH, 3-ONO_2)-IHN ratio. Data points are the means and the shaded areas represent ±1 s.d. in the variability of values for each hour of the day.

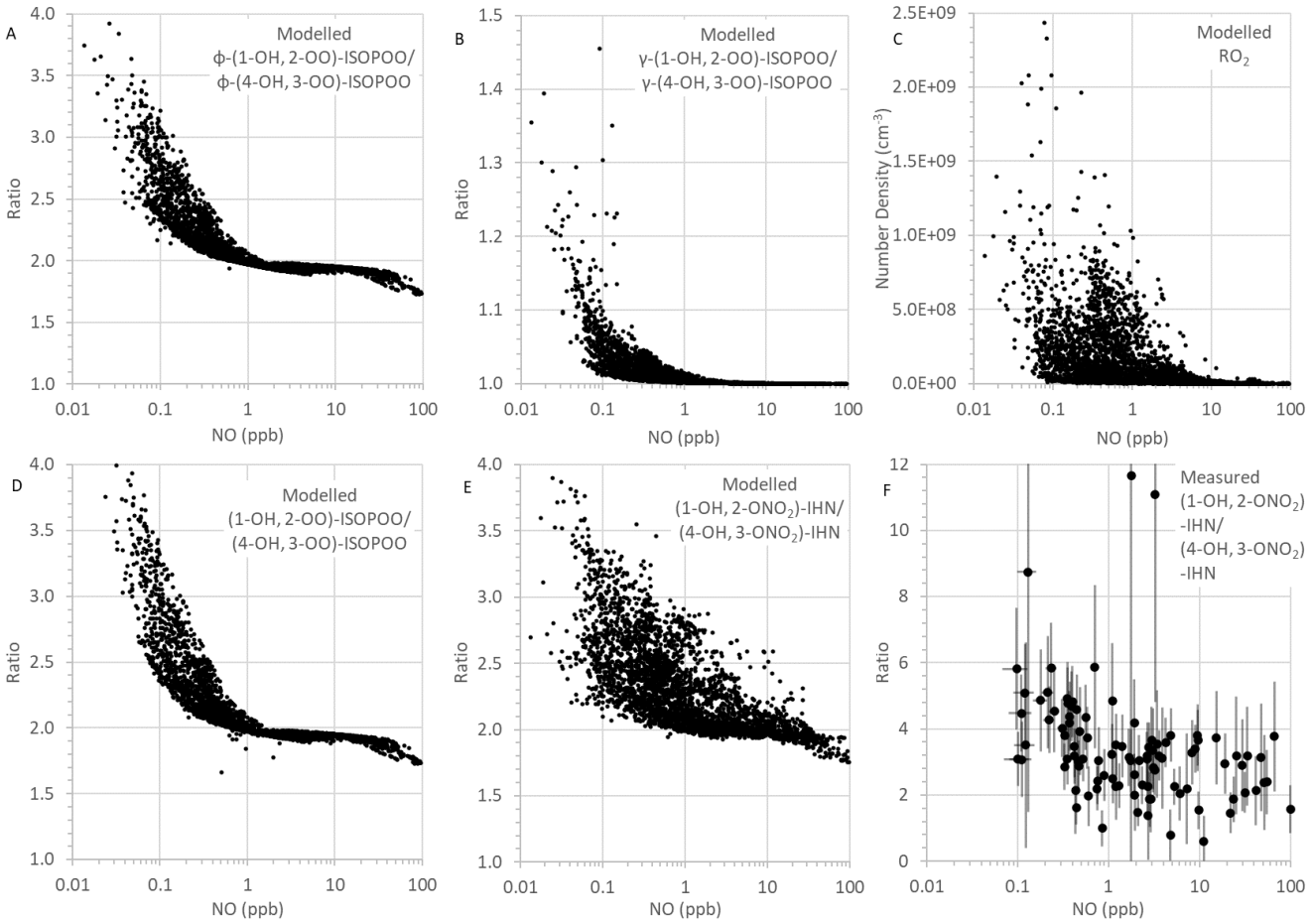

Figure 7: MCM modelled and measured parameters as a function of NO mixing ratio: (a) Modelled ratio of φ-(1-OH, 2-OO)-ISOPOO to φ- (4-OH, 3-OO)-ISOPOO; (b) Modelled ratio of γ-(1-OH, 2-OO)-ISOPOO to γ-(4-OH, 3-OO)-ISOPOO; (c) Modelled RO_2 number density; (d) Modelled ratio of (1-OH, 2-OO)-ISOPOO to (4-OH, 3-OO)-ISOPOO; (e) Modelled ratio of (1-OH, 2-ONO_2)-IHN to (4-OH, 3-ONO_2)-IHN; (f) Measured ratio of (1-OH, 2-ONO_2)-IHN to (4-OH, 3-ONO_2)-IHN (error bars are the measurement uncertainties (see Sect. 3.3 for details)).

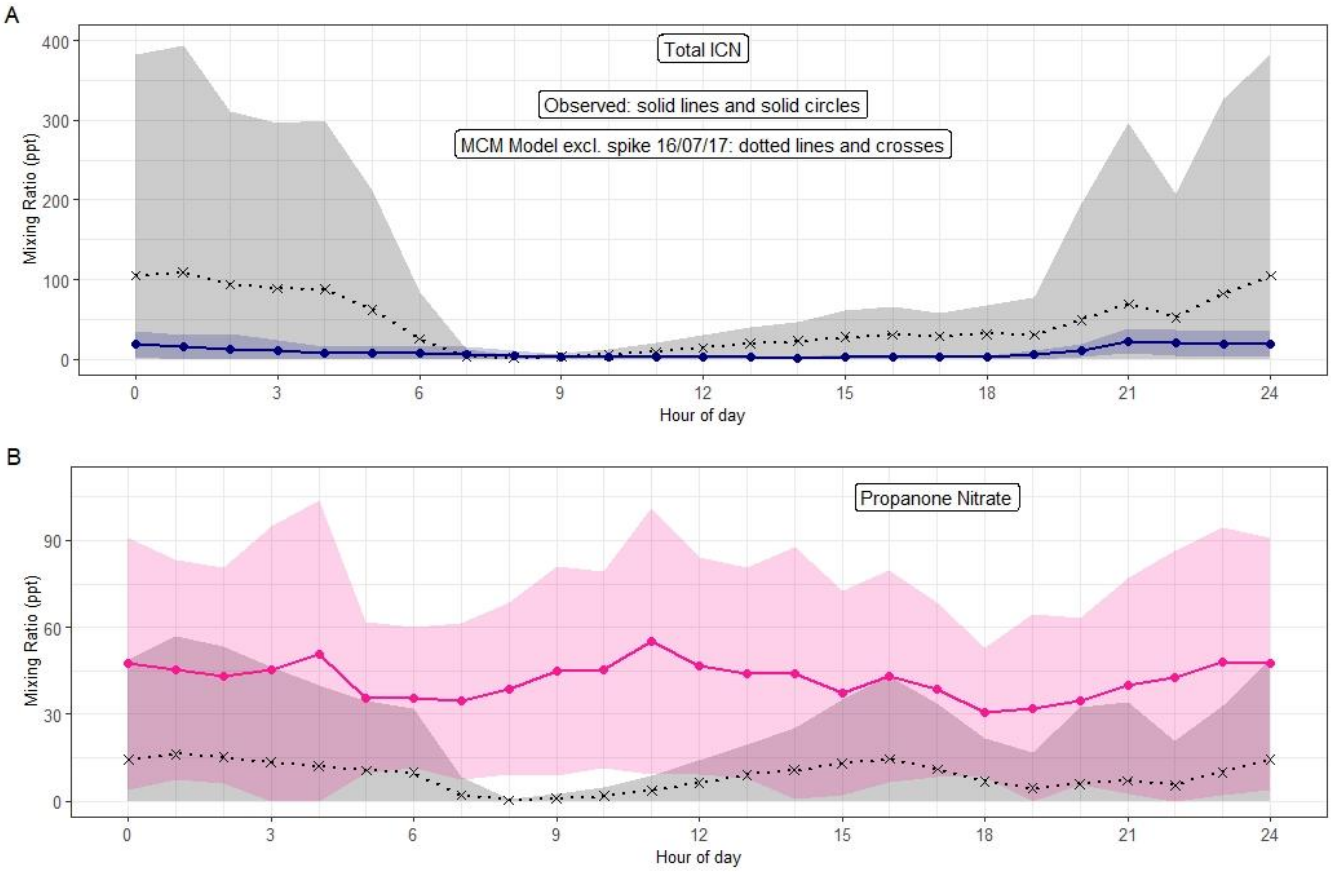

Figure 8: (a) Diel pattern of total ICN as modelled using the MCM and measured. For the MCM this is the specie NC4CHO, whilst the measurements are the sum of the four δ-ICN (E and Z-(1-ONO_2, 4-CO)-ICN and E and Z-(4-ONO_2, 1-CO)-ICN). (b) Diel pattern of propanone as modelled using the MCM and measured. Data points are the means and the shaded areas represent ±1 s.d. in the variability of values for each hour of the day.

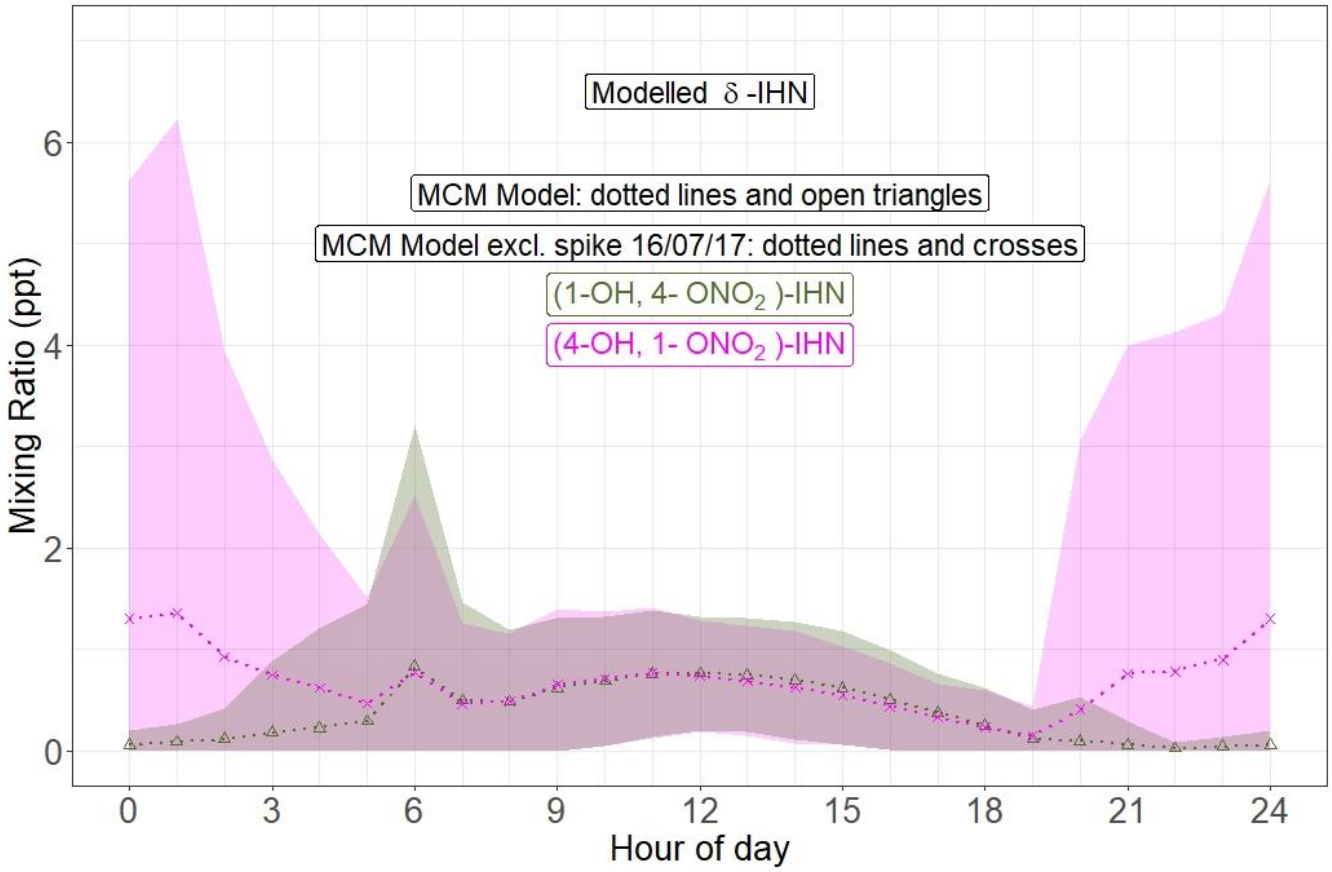

905

Figure 9: Diel pattern of MCM modelled δ-IHN ((1-OH, 4-ONO_2)-IHN and (4-OH, 1-ONO_2)-IHN). Data points are the means and the shaded areas represent ±1 s.d. in the variability of values for each hour of the day.